VOL. 258 SUMMER 1960 No. 7

American Journal of Science

Established in 1818 by Benjamin Silliman

EDITORS
JOHN RODGERS—JOSEPH T. GREGORY

ASSOCIATE EDITORS

GEORGE GAYLORD SIMPSON, CAMBRIDGE, MASS.
A. F. BUDDINGTON, PRINCETON, N. J.
CARL O. DUNBAR
HENRY MARGENAU
HORACE WINCHELL
EDWARD S. DEEVEY, JR.
MATT WALTON
RICHARD F. FLINT
HAROLD G. CASSIDY
G. EVELYN HUTCHINSON
NEW HAVEN, CONN.
WILMOT H. BRADLEY
PHILIP H. ABELSON
WASHINGTON, D. C.
LEASON H. ADAMS, LOS ANGELES, CALIF.
HOWEL WILLIAMS, BERKELEY, CALIF.
C. R. LONGWELL, PALO ALTO, CALIF.
ADOLPH KNOPF, STANFORD, CALIF.
FREDERICK J. ALCOCK, OTTAWA, CANADA
CECIL E. TILLEY, CAMBRIDGE, ENGLAND

STERLING TOWER
YALE UNIVERSITY
NEW HAVEN, CONNECTICUT

Published 10 times a year. Ten dollars a year. One dollar twenty-five cents a copy.
Foreign, ten dollars sixty cents. Canada, ten dollars thirty-five cents.

AMERICAN JOURNAL OF SCIENCE

Established in 1818 by Benjamin Silliman

THE FIRST SCIENTIFIC JOURNAL IN THE UNITED STATES

DEVOTED TO THE GEOLOGICAL SCIENCES AND TO RELATED FIELDS

Editors: JOHN RODGERS—JOSEPH T. GREGORY
Managing Editor: BETH A. BROMBERT

Entered as second-class matter at the Post Office at New Haven, Conn., under the Act of March 3, 1879. Published monthly, except July and September, at Sterling Tower, Yale University, New Haven, Conn.

Subscription rate $10 per year ($1.25 a number). Student rate $5 per year (application blanks available on request). Postage prepaid to the United States; 35 cents per year to Canada; 60 cents per year elsewhere.

The JOURNAL completed its *first* series of 50 volumes in 1845, its *second* series of 50 volumes in 1870, its *third* series of 50 volumes in 1895, its *fourth* series of 50 volumes in 1920, its *fifth* series of 36 volumes in 1938. Since 1938 the numbering by series has been discontinued, and volumes are annual and bear the whole numbers as of 1818, that for 1939 being volume 237.

Back numbers and volumes, also cumulative indices of all series, may with few exceptions be obtained from the office of the AMERICAN JOURNAL OF SCIENCE, Sterling Tower, New Haven, Conn. Positive microfilm copies of each complete volume may be purchased by subscribers to the paper edition from *University Microfilms*, 313 N. First St., Ann Arbor, Michigan. Regular subscribers may purchase each past year in microcard form, from *The Microcard Foundation*, Wesleyan University, Middletown, Connecticut.

INSTRUCTIONS TO CONTRIBUTORS

Typescripts of articles submitted should be double-spaced, should follow the recommendations in the pamphlet *Suggestions to Authors*, 5th ed. (see below), and should be preceded by brief abstracts. They should be checked with special care before being submitted, to avoid changes in proof other than printer's errors.

References to literature should be listed alphabetically by authors at the end of the article; all references should be complete. For articles in journals or other serial publications, the reference should give in order: Author's name, year of publication, full title: name of periodical or series, volume number, inclusive pages. For books or other unnumbered publications, it should give: Author's name, years of publication, full title: place of publication, publisher. This form follows the recommendations in the pamphlet "Abbreviations used in publications of the U. S. Geological Survey", which is also the standard used for abbreviating names of periodicals, etc. Citations within an article should be to author and year, with specific pages wherever appropriate.

Plates (photographs), *figures* (line drawings), and *footnotes* should each be numbered consecutively through each article, using arabic numerals. If two photographs form one plate, they are figures 1 and 2 of that plate.

Illustrations should be neat and legible and should include explanations of symbols used. Copy that cannot be reproduced cannot be accepted. Plates and figures should be capable of reduction to not more than 4 by 7 inches, all lettering being at least 1/16th inch high after reduction. When necessary, one large map or table can be accepted, if it will not exceed 7 inches in width after reduction. Line drawings should be in black India ink on white drawing board, tracing cloth, or coordinate paper printed in blue. Photographs should be positive glossy prints. Photostatic and typewritten material cannot be accepted as copy for illustrations.

Reprints. Thirty separate copies of each article will be furnished to the author free of cost and without previous notice from him; these will be without a cover. Additional copies will be furnished at cost, which will of course be greater if the article is accompanied by plates involving unusual expense. Copies will be furnished with a printed cover giving the title, author, volume, page, and year, when specially ordered.

Suggestions to Authors of the Reports of the United States Geological Survey, 5th ed. Washington, D. C., 1958 (Government Printing Office, $1.75).

[American Journal of Science, Vol. 258, Summer 1960, P. 449-497]

American Journal of Science
SUMMER 1960

COMPOSITIONAL CHARACTERISTICS AND EQUILIBRIUM RELATIONS IN MINERAL ASSEMBLAGES OF A METAMORPHOSED IRON FORMATION

ROBERT F. MUELLER

Scripps Institution of Oceanography, La Jolla, California

ABSTRACT. The iron formation is located in east-central Quebec and probably is a regionally metamorphosed equivalent of the iron-bearing sediments of the Labrador trough. Mineral assemblages are composed of select combinations of the following: quartz, talc, actinolite, Ca-pyroxene, cummingtonite, magnetite, hematite, calcite, and dolomite. Seventy-six spectrographic analyses of minerals give the following average concentration ranges for minor constituents: Al_2O_3, MnO, and Na_2O <1%; K_2O <0.1%; TiO_2, V_2O_5, Cr_2O_3, NiO, CuO, and BaO <0.01%. ZrO_2 and SrO were not detected. Therefore the rocks are essentially members of the system $CaO–MgO–FeO–O–SiO_2–H_2O–CO_2$.

Close approach to chemical equilibrium during metamorphism is indicated by (1) orderly distribution of Mg, Fe, and Mn among coexisting actinolite, Ca-pyroxene, and cummingtonite; (2) restrictions on the numbers and types of minerals in association with each other; and (3) correlation of the compositions of silicates with the presence and absence of hematite, i.e., Mg/(Mg + Fe) is increased and its range restricted when hematite is present.

Distributions of elements among coexisting minerals may be interpreted in terms of thermodynamic theory and in some cases may be represented by functions derived on the assumption of ideal solid solutions. Observed mineral assemblages and their compositional relations are in general consistent with phase rule considerations and may be elucidated by functions based on the coupling of chemical reactions between minerals.

INTRODUCTION

Goldschmidt (1911) made the first attempt to relate metamorphic mineral assemblages to the restrictions imposed upon them by thermodynamics. His observations led him to propose the mineralogical phase rule. The fact that many metamorphic rocks are found to obey this rule provides evidence for the prevalence of equilibrium conditions. However, this conclusion must be weighed in terms of kinetic factors as was done by Harker (1932) when he wrote:

> . . . the 'system' for which Goldschmidt's adaptation of the phase rule may hold good is not the rock as a whole, but merely any portion of it small enough to be comprised within the sphere of free diffusion.

This observation is of great importance to the study of mineral assemblages.

In order to understand in detail the factors which contribute to the origin of a particular mineral assemblage, the compositions of coexisting minerals must be known and the possible chemical reactions between different minerals evaluated. The significance of mineral compositions and the interactions of mineral phases have been stressed by Ramberg (1952). In the present study the phase rule of Gibbs is used as a guide in explaining the variations shown by the assemblages. An attempt is made, within the framework of simplifying assumptions, to evaluate the chemical reactions between minerals and between minerals and a postulated gaseous phase. An attempt is also made to relate the compositions of coexisting minerals to their solid solution properties, to the

presence or absence of certain phases, and to the conditions during metamorphism. Since the thermal properties of the minerals studied are only imperfectly known, the interpretation is concerned with the derivation of general relationships rather than the determination of absolute values of temperatures and pressures of crystallization.

This study was begun during the summers of 1956 and 1957 while the writer was in Quebec as an employee of the Jones and Laughlin Steel Corporation. The Quebec iron formation seems suited to a study of this kind because it is a system of intermediate complexity and provides an opportunity to observe the influence of oxidation during metamorphism.

MINERAL SEPARATION AND ANALYTICAL METHODS

The minerals were separated with a Frantz isodynamic separator and by hand-picking when necessary. Most minerals were washed in a solution of approximately 5 percent HCl to remove carbonates. In the case of rocks which contained magnetite as the only abundant iron oxide phase, it was found possible to eliminate the greater part of the oxide inclusions by magnetic means. For hematite-bearing rocks this was not possible; therefore all the silicates which coexisted with hematite were hand-picked under a microscope and every visible oxide inclusion was in this manner removed. Inclusions of other minerals are estimated at less than 2 percent. Because of the generally low calcium content of cummingtonites, a considerable proportion of their measured calcium (table 1) probably represents inclusions of minerals rich in this element.

The spectrographic analyses were done by the writer using a method developed by Oiva I. Joensuu. The spectrographic equipment and the analytical procedure as applied to carbonates have been described by Goldsmith, Graf, and Joensuu (1955). For the silicate analyses the method as described by these authors was modified as follows: Sample electrodes were made from 1/8 inch no. 5185 United Carbon Products Company graphite rods with a 1/16 inch diameter hole drilled to a depth of 12 mm. The counter electrode was a 3/16 inch carbon rod sharpened with a pencil sharpener. During arcing the current was kept adjusted to 10 amperes. A Co internal standard consisting of 20 percent Co_3O_4 mixed with Li_2CO_3 was used for all the silicate analyses. In preparation of the sample one part of the internal standard was mixed with 10 parts of the mineral, 30 parts of Li_2CO_3, and 40 parts H_3BO_3. This mixture was fused at 900°C for twenty minutes. The resulting bead was crushed and ground. One part of this powder was then mixed with two parts of graphite powder. Two electrodes for each sample were filled and arced to completion. The working curves for the silicates were prepared from a wide variety of mineral and rock standards.

For the four analyses of magnetite and hematite (table 2) no internal standard was added. Since these oxides contain few impurities the amount of iron they contain is practically constant. Therefore the iron of these oxides may be used as an internal standard. Working curves were prepared from analyzed magnetite standards to which known amounts of the various oxides had been added. The iron line intensities were corrected for the dilution effect of these oxides. All samples were prepared by mixing one part magnetite or hematite

powder with four parts of graphite. Standard electrodes as described above were filled and arced.

The precision of the spectrographic method as used is approximately ± 5 percent of the amount present for Al_2O_3, Fe, MnO and MgO over the greater part of the concentration ranges encountered. However, for many specimens Al_2O_3 was determined only to an order of magnitude. Also, for the determinations near the limit of measurement (indicated by the symbol "<" in the tables) the precision diminishes to an order of magnitude of the amount present. This is the case for most of the determinations of TiO_2, V_2O_3, Cr_2O_3, NiO, CuO, and BaO. However, for the higher concentrations of TiO_2 the precision is approximately ± 5 percent. For SiO_2 generally and for CaO in the concentration range of actinolite or lower the precision is approximately ± 10 percent. For CaO in the concentration range of Ca-pyroxene the precision is about ± 20 percent. Na_2O and K_2O were determined by means of a Beckman Model DU spectrophotometer with flame attachment. The precision is approximately ± 5 percent for most of the determinations but diminishes to an order of magnitude near the limit of measurement at 0.01 percent.

Mineral phases were identified by optical examination of thin sections and granular aggregates, x-ray diffraction method, and by observing the behavior of grains in the magnetic field. Magnetite and hematite were found to be readily distinguishable in thin section because of their generally coarse grain sizes and the color of their reflecting surfaces. The possible existence of fine intergrowths of hematite in magnetite was not investigated. Thus in assemblages for which hematite is not listed as a phase, the possibilities of such occurrences cannot be excluded. However, hematite other than stains along grain boundaries and cleavages was never observed in these assemblages. Also, in these assemblages no hematite was observed in x-ray diffractometer patterns of magnetite or during the course of magnetic separation of the minerals.

Fine-grained limonite, hematite, and probably other alteration products occur as stains along cleavages and between grains, but the quantity of this material is minute. Because of its fine-grained nature as compared with the metamorphic minerals, this material is interpreted as a late alteration product and is omitted from further consideration.

THE GEOLOGIC SETTING OF THE IRON FORMATION

Location.—The iron formation is located approximately 180 miles north of Seven Islands, Quebec, near the Labrador boundary (fig. 1) and probably represents a southwestern extension of the iron-bearing sediments of the Labrador Trough. It appears to be part of the same general belt as that at Mt. Wright, a few miles to the south, which has been described by Gross (1955).

The specimens used in this study were collected from an area of several square miles lying between Mogridge and Golden Lakes and bounded on the east by Bloom Lake. Specimens designated "DH" are from drill cores. The hole numbers and footages are also given. Other numbers refer to specimens collected from surface exposures.

Geology.—The iron formation is a very subordinate part of a complex of Precambrian metasediments and meta-igneous rocks. Schists, consisting of

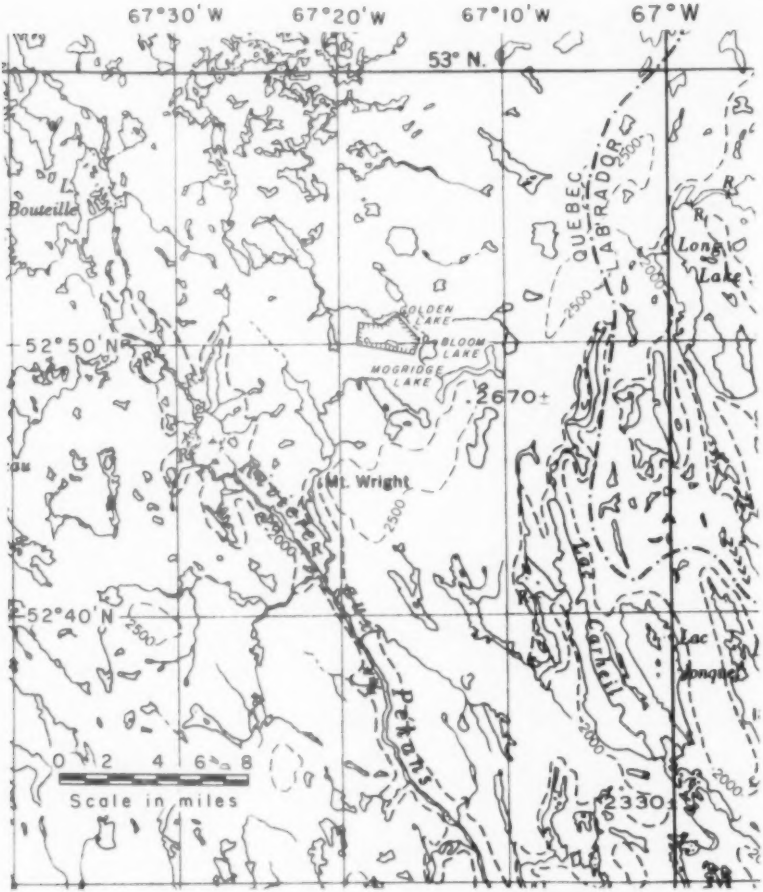

Fig. 1. Location of the Quebec iron formation. All specimens come from areas shown by hatched borders near the center of the map.

biotite, muscovite, quartz, feldspar, hornblende, garnet, and epidote dominate in areal extent. Dips of compositional banding and the conformable plane of major schistosity are generally steep. In some areas the schists inclose lens-shaped concordant bodies of granite several hundreds of feet in greatest dimension which usually contain the same minerals as the enveloping schists. These granites were not observed in the iron formation. These relations suggest that the granites may be metamorphic in origin and that their constituents were derived from the schists.

Within the schists lie the conformable bodies of iron formation ranging in thickness from less than one hundred to over a thousand feet. Though

thoroughly metamorphosed, the iron formation retains a banded character frequently resembling the iron-bearing sediments of the Lake Superior region. This feature and the general stratigraphic relations of the iron formation bodies to the mica schists strongly suggest a sedimentary origin. The detailed chemistry (discussed in the next section) indicates that the iron formation was chemically deposited in the form of silica and calcium, magnesium, and iron carbonates and perhaps some iron oxides. These rocks, which are very low in aluminum, show knife-sharp contacts with the mica schists. The contacts appear to mark a sharp compositional change during sedimentation.

Within the iron formation various members were distinguished in the field as a consequence of distinctive mineral associations and differences in the proportions of certain minerals. These members in general appear to form a stratigraphic sequence, although deformation and metamorphism have obscured most of the original features of the stratigraphy. Laboratory work has shown that some of the members coincide with the groups of mineral assemblages designated "A" and "B" (table 4) which are significant with respect to the thermodynamic conditions of metamorphism. The most widespread assemblage of the B group is represented by the association actinolite-talc-magnetite-hematite-carbonate-quartz. Equally widespread are the assemblages of the A group which are composed of various combinations of cummingtonite, Ca-pyroxene (diopside-hedenbergite), actinolite, magnetite, carbonate, and quartz.

Structural features of the iron formation suggest the sequence of events during metamorphism. Banding is sharply defined by segregations of coarse ferromagnesian silicates and quartz. Quartz-rich bands are frequently broken into lens-shaped fragments which are rotated. Where these bands reach thicknesses of six inches or more they commonly show the familiar S-shaped fractures of competent beds. These fractures are filled with unfractured amphiboles which appear to have been derived from adjacent amphibole-rich bands, indicating that fracturing preceded crystallization. These relations indicate that the amphiboles of the amphibole-rich layer or the substance from which the amphiboles were derived was plastic at the time of fracturing. It seems most probable that this plastic substance was a mixture of the various carbonates, which gave rise, by reacting with quartz, to the amphiboles and other ferromagnesian silicates.

Steeply plunging open folds are common in members containing the B group assemblages. These folds are of several orders of dimension and show systematic relations to each other and the S-shaped fractures. Actinolite is commonly oriented parallel to the fold axes. Folding in the A group of assemblages is usually more complex and chaotic.

Sills or crosscutting irregular bodies of amphibolite occur in the iron formation and on its edges. Compositional banding and schistosity in the amphibolite are parallel to those of the iron formation, even when the amphibolite cuts the iron formation bands at 90°. This shows that the two rocks underwent the same culminating metamorphism. The amphibolite consists of hornblende, biotite, plagioclase (An_{25}-An_{35}), quartz, garnet, scapolite, epidote, apatite, and oxides. Field evidence indicates that the amphibolite has been

derived from an olivine biabase, some of which still remains in the larger bodies of amphibolite. This diabase contains clinopyroxene and sharply zoned plagioclase.

There appear to be no well-defined contact effects of the diabase on the iron formation. There is a tendency for group A assemblages to occur near contacts with the amphibolite, but these also occur at a distance. In all probability most of the original contact effects of the diabase, if any, were obliterated by the subsequent general recrystallization.

CHEMICAL CHARACTERISTICS OF THE IRON FORMATION

Bulk chemistry.—The composition of the iron formation approximates closely the system CaO–MgO–FeO–O–SiO_2–H_2O–CO_2. Because of the banding of the rocks it is difficult to speak of the composition of rock specimens except in the broadest terms. However, for the iron formation as a whole the mineral composition in order of decreasing volumetric importance appears to be quartz, ferromagnesian silicates, iron oxides, and carbonates. The effective concentrations of the elements in any given specimen are best revealed by the compositions of the minerals given in tables 1 and 2 and the list of mineral assemblages in table 4. These data show the dominance of the seven major constituents.

The silicate mineral analyses of table 1 show that among the minor oxides only MnO and Al_2O_3 surpass one per cent, although their averages lie below this level. Na_2O approaches one percent in only a few actinolites and pyroxenes. The average content of TiO_2 appears to be less than 0.01 percent in the ferromagnesian silicates, and the contents of ZrO_2, V_2O_3, Cr_2O_3, NiO, CuO, SrO, and BaO undoubtedly lie well below this level. Of these oxides ZrO_2 and SrO were not detected, although CuO and BaO frequently appeared below the limits of measurement. K_2O was detected in nearly all the specimens which were analyzed for this oxide, but it appears to average only several hundredths of a percent.

A notable feature is the relatively high content of manganese of many of the cummingtonites. Cummingtonite is the dominant ferromagnesian silicate of the A group of assemblages and may in some specimens comprise more than 50 percent of the rock. Consequently the manganese content of this group is probably higher as an average than that of the B group. It is possible that the original stratigraphic members represented by the two groups differed in this respect.

Four incomplete analyses of iron oxides from the iron formation (table 2) indicate low concentrations for all the minor elements determined. TiO_2 and MnO appear to be present in even lower concentrations than in the coexisting silicates.

If the ferromagnesian silicates contain most of the minor elements, as they appear to, rocks consisting of varying proportions of these silicates to quartz and iron oxides will have even lower concentrations of minor elements than if they were composed of the pure ferromagnesian silicates. It is interesting to compare such "possible" Quebec iron formation rocks with iron-bearing rocks from other areas. Rankama and Sahama (1949) have tabulated Ti, V, Cr, Mn, and Ni contents for such rocks. When these tabulated values are compared with

TABLE 1

Spectrochemical analyses of silicate minerals

	Actinolite								
	DH3–172	B-13	DH10–158	B-22	B-20	DH7-445	12BA	12AB	DH10-101
SiO_2	51.0	51.0	53.0	55.0	55.0	52.0	55.0	52.0	55.0
TiO_2	< 0.01	0.032	< 0.01	0.010	< 0.01	< 0.01	0.050	0.046	< 0.01
Al_2O_3	~0.6	nd	~0.2	0.40	nd	~0.3	~0.6	~1.0	~0.9
Fe	17.0	21.0	14.0	11.0	12.5	11.0	14.0	15.5	7.3
Fe_2O_3	nd	nd	nd	nd	nd	nd	nd	nd	nd
FeO	21.9	27.0	18.0	14.2	16.1	14.2	18.0	20.0	9.4
MnO	0.78	0.20	0.29	0.31	0.26	0.71	0.29	0.37	0.62
MgO	9.7	6.1	13.5	18.0	14.0	15.0	11.0	11.5	20.5
CaO	10.0	10.5	10.0	11.0	10.0	10.5	10.0	11.0	10.0
Na_2O	nd	nd	nd	nd	nd	0.08	0.24	nd	0.78
K_2O	nd	nd	nd	nd	nd	0.04	0.04	nd	0.02
ZrO_2	———	———	———	———	———	———	———	———	———
V_2O_3	———	———	———	———	———	———	0.011	0.014	———
Cr_2O_3	———	———	———	———	———	———	———	———	———
NiO	———	———	———	———	———	———	———	———	———
CuO	nd	nd	nd	nd	nd	< 0.005	nd	< 0.005	nd
SrO	———	———	———	———	———	———	———	———	———
BaO	———	< 0.01	< 0.01	———	< 0.01	nd	———	< 0.01	———

"<" indicates that the oxide or element is present but below the limit of measurement given.

"~" indicates an approximate value.

——— indicates that the element was looked for but not found.

"nd" indicates that the element was not determined.

FeO was determined for one specimen by Mr. Edward J. Olsen; for all other specimens FeO is calculated from total Fe.

TABLE 1 (Cont.)

	Actinolite								
	9G	G-15	F-1	2G	4G	8G	Dr-1	14G	DHI-21
SiO_2	55.0	54.0	56.0	58.0	56.0	55.0	51.0	52.0	49.0
TiO_2	< 0.01	———	———	0.16	0.031	0.015	0.020	< 0.01	< 0.01
Al_2O_3	~0.2	~0.1	0.22	~0.5	~0.4	~0.2	~0.6	< 0.1	~0.4
Fe	9.4	11.0	6.4	4.7	4.6	4.5	4.3	4.5	4.3
Fe_2O_3	nd	nd	nd	nd	nd	nd	nd	0.2	nd
FeO	12.1	14.2	8.2	6.0	5.9	5.8	5.5	5.6	5.5
MnO	0.60	0.79	0.11	0.59	0.23	0.30	0.41	0.43	0.27
MgO	17.5	15.5	22.0	22.0	21.0	22.0	22.5	21.0	21.0
CaO	12.0	12.0	11.0	12.5	12.0	12.5	11.0	13.0	11.0
Na_2O	0.60	nd	nd	nd	nd	nd	nd	0.20	nd
K_2O	0.08	nd	nd	nd	nd	nd	nd	0.03	nd
ZrO_2	———	———	———	———	———	———	———	———	———
V_2O_3	———	———	———	———	———	———	———	———	———
Cr_2O_3	———	———	———	———	———	———	———	———	———
NiO	———	———	———	———	———	———	———	———	———
CuO	< 0.005	nd	nd	< 0.005	< 0.005	< 0.005	nd	nd	nd
SrO	———	———	———	———	———	———	———	———	———
BaO	< 0.01	———	———	< 0.01	< 0.01	< 0.01	0.016	———	———

TABLE 1 (Cont.)

	Actinolite								Ca-py
	DH1–32	DH1–52	DH4–185	DH7–480	DH11-200	10G	DH13-607	DH7-291	B-15
SiO_2	51.0	54.0	55.0	52.0	55.0	56.0	52.0	53.0	51.0
TiO_2	0.030	< 0.01	< 0.01	< 0.01	< 0.01	———	< 0.01	< 0.01	0.015
Al_2O_3	~0.7	0.46	~0.9	~0.8	0.35	1.2	~0.2	~0.2	nd
Fe	4.6	4.4	5.1	5.0	4.3	4.5	4.7	3.2	18.0
Fe_2O_3	nd	nd	nd	nd	nd	nd	nd	nd	nd
FeO	5.9	5.7	6.6	6.4	11.5	11.0	12.5	12.5	23.2
MnO	0.29	0.25	0.47	0.43	nd	0.58	nd	nd	0.42
MgO	21.0	21.5	20.0	21.0	nd	0.07	nd	nd	4.6
CaO	11.5	13.0	11.0	11.0	5.5	5.8	6.0	4.1	19.0
Na_2O	nd	nd	0.44	0.42	0.38	0.25	0.48	0.39	nd
K_2O	nd	nd	0.04	0.05	22.0	22.0	21.0	23.0	nd
ZrO_2	———	———	———	———	———	———	———	———	———
V_2O_3	———	———	———	———	———	< 0.008	———	———	———
Cr_2O_3	———	———	———	———	———	———	———	———	———
NiO	———	———	———	———	———	———	———	———	———
CuO	nd	nd	nd	nd	nd	nd	nd	nd	nd
SrO	———	———	———	———	———	———	———	———	———
BaO	———	———	———	———	———	———	< 0.01	———	< 0.01

TABLE 1 (Cont.)

	Ca-pyroxene								
	DH3–172	DH9–324	DH10–169	2B	B-13	B-16	DH3-149	CL-1	6B
SiO_2	49.0	47.0	50.0	49.0	48.0	48.0	50.0	50.0	51.0
TiO_2	< 0.01	< 0.01	0.025	< 0.01	< 0.01	< 0.01	< 0.01	< 0.01	< 0.01
Al_2O_3	~0.4	nd	~0.3	~0.3	nd	nd	~0.3	nd	~0.5
Fe	13.5	16.0	16.5	19.5	17.0	19.0	15.0	16.0	16.5
Fe_2O_3	nd	nd	nd	nd	nd	nd	nd	nd	nd
FeO	17.4	20.6	21.2	25.1	21.9	24.4	19.3	20.6	21.2
MnO	0.90	1.10	0.64	0.44	0.25	0.39	1.25	0.46	0.34
MgO	7.2	5.8	5.2	1.8	5.6	3.9	6.2	6.0	5.7
CaO	19.0	19.0	19.0	22.0	19.0	18.0	18.0	19.0	21.0
Na_2O	nd	0.34	nd	0.11	nd	nd	nd	nd	nd
K_2O	nd	0.02	nd	0.07	nd	nd	nd	nd	nd
ZrO_2	———	———	———	———	———	———	———	———	———
V_2O_3	———	0.008	———	———	———	———	———	< 0.008	———
Cr_2O_3	———	———	———	———	———	———	———	———	———
NiO	———	———	< 0.01	———	———	———	———	———	———
CuO	nd	< 0.005	nd	< 0.005	nd	< 0.005	nd	nd	< 0.005
SrO	———	———	———	———	———	———	———	———	———
BaO	———	nd	< 0.01	< 0.01	< 0.01	nd	———	———	< 0.01

TABLE 1 (Cont.)

	Ca-pyroxene							Cummingtonite	
	B–14	DH5–77	B–20	3B	DH7-445	12BA	DH13-607	B-15	DH3-172
SiO_2	52.0	52.0	51.0	50.0	50.0	47.0	57.0	52.0	50.0
TiO_2	< 0.01	0.015	nd	0.020	< 0.01	< 0.01	< 0.01	0.020	0.01
Al_2O_3	~0.3	~1.5	nd	~0.3	~0.3	~0.3	~0.3	nd	~0.4
Fe	19.0	16.0	10.5	13.5	9.3	12.5	4.2	31.0	24.5
Fe_2O_3	nd	nd	nd	nd	nd	nd	nd	nd	nd
FeO	24.4	20.6	13.5	17.4	12.0	16.1	5.4	39.9	31.5
MnO	0.41	1.35	0.30	0.35	0.82	0.33	0.56	0.75	1.55
MgO	3.8	6.5	10.5	9.0	12.5	8.5	16.0	5.5	8.8
CaO	22.0	20.0	21.0	19.0	22.0	19.0	20.0	0.90	1.9
Na_2O	nd	0.36	nd	0.80	0.10	0.38	nd	nd	nd
K_2O	nd	0.02	nd	0.08	0.02	0.03	nd	nd	nd
ZrO_2	———	———	———	———	———	———	———	———	———
V_2O_3	< 0.008	< 0.008	———	0.01	———	0.018	< 0.008	———	———
Cr_2O_3	———	———	———	———	———	———	———	———	———
NiO	———	———	———	0.01	———	———	———	———	———
CuO	< 0.005	< 0.005	nd	< 0.005	< 0.005	nd	nd	nd	nd
SrO	———	———	———	———	———	———	———	———	———
BaO	< 0.01	< 0.01	< 0.01	< 0.01	nd	———	< 0.01	———	———

TABLE 1 (Cont.)

	Cummingtonite									
	DH3-324	DH10-169	2B	B-13	B-16	DH3-149	CL-1	6B	B-14	
SiO_2	49.0	50.0	49.0	50.0	48.0	50.0	54.0	53.0	51.0	
TiO_2	0.011	< 0.01	———	0.018	< 0.01	< 0.01	0.022	< 0.01	———	
Al_2O_3	~0.2	~0.2	~0.2	nd	~0.5	~0.5	nd	< 0.1	~0.2	
Fe	27.0	28.5	32.0	30.0	30.0	27.0	30.0	28.5	31.5	
Fe_2O_3	nd	nd	nd	nd	nd	nd	nd	nd	nd	
FeO	34.7	36.7	41.2	38.6	38.6	34.7	38.6	36.7	40.5	
MnO	1.8	1.05	0.68	0.53	0.68	2.1	0.83	0.63	0.69	
MgO	7.2	7.2	3.0	6.0	4.4	7.6	7.3	8.5	4.3	
CaO	0.70	0.78	1.0	0.81	1.1	1.3	0.75	0.95	1.0	
Na_2O	0.02	nd	0.02	nd	nd	nd	nd	nd	nd	
K_2O	0.02	nd	0.02	nd	nd	nd	nd	nd	nd	
ZrO_2	———	———	———	———	———	———	———	———	———	
V_2O_3	———	———	———	———	———	———	———	< 0.01	———	
Cr_2O_3	———	———	———	———	———	———	———	< 0.01	———	
NiO	———	———	———	———	< 0.005	nd	nd	< 0.005	< 0.005	
CuO	< 0.005	nd	0.008	nd	———	———	———	———	———	
SrO	———	———	———	———	———	———	———	———	———	
BaO	nd	< 0.01	———	———	nd	———	———	< 0.01	———	

TABLE 1 (Cont.)

	Cummingtonite								
	DH5–77	DH10–131	DH10–158	B-19	DH7–484	DH10–95	B–22	B–22A	DH10–78
SiO_2	50.0	51.0	51.0	48.0	54.0	53.0	55.0	54.0	54.0
TiO_2	< 0.01	———	< 0.01	< 0.01	< 0.01	———	< 0.01	< 0.01	———
Al_2O_3	~0.4	~0.2	~0.2	~0.3	nd	0.15	~0.1	0.29	~0.2
Fe	27.5	26.5	22.0	29.0	20.0	19.0	17.5	25.0	21.0
Fe_2O_3	nd	nd	nd	nd	nd	nd	nd	nd	nd
FeO	35.4	34.1	28.3	37.3	25.7	24.4	22.5	32.2	27.0
MnO	2.05	1.6	0.85	0.63	1.40	1.7	0.55	0.47	1.05
MgO	7.5	8.4	11.5	6.4	15.0	16.0	15.0	10.5	15.0
CaO	0.70	0.63	1.0	0.73	0.53	1.0	2.5	0.65	0.50
Na_2O	0.08	0.05	nd	nd	nd	nd	0.02	0.06	nd
K_2O	0.03	0.03	nd	nd	nd	nd	———	0.03	nd
ZrO_2	———	———	———	———	———	———	———	———	———
V_2O_3	———	———	———	———	———	———	———	———	———
Cr_2O_3	———	———	———	———	———	———	———	———	———
NiO	———	———	———	———	———	———	———	———	———
CuO	< 0.005	< 0.005	nd	< 0.005	nd	nd	nd	nd	< 0.005
SrO	———	———	———	———	———	———	———	———	———
BaO	nd	nd	< 0.01	nd	———	———	———	———	———

TABLE 1 (Cont.)

	Cummingtonite								
	DH7–482	7B	1B	8B	9B	B–17	DH7–490	DH10–85	10G
SiO_2	48.0	51.0	48.0	50.0	52.0	49.0	54.0	46.0	nd
TiO_2	< 0.01	———	———	< 0.01	< 0.01	———	———	———	nd
Al_2O_3	0.40	~0.2	< 0.1	~0.2	< 0.1	< 0.1	0.15	0.30	~0.5
Fe	15.5	26.5	36.0	35.5	35.5	34.0	20.0	22.0	9.6
Fe_2O_3	nd	nd	nd	nd	nd	nd	nd	nd	nd
FeO	20.0	34.1	46.3	45.6	45.6	43.8	25.7	28.3	12.3
MnO	1.35	0.55	0.57	1.25	1.10	0.79	1.40	1.45	0.80
MgO	18.5	10.5	0.52	0.65	1.4	2.3	13.5	12.0	23.0
CaO	2.2	1.0	0.65	0.51	0.65	0.70	0.45	2.5	1.1
Na_2O	nd	nd	nd	0.02	0.30	nd	nd	nd	nd
K_2O	nd	nd	nd	0.02	0.18	nd	nd	nd	nd
ZrO_2	———	———	———	———	———	———	———	———	———
V_2O_3	———	———	———	———	———	———	———	———	———
Cr_2O_3	———	———	———	———	< 0.01	———	———	———	———
NiO	———	———	———	———	< 0.01	———	———	———	———
CuO	nd	< 0.005	nd	< 0.005	< 0.005	nd	nd	nd	nd
SrO	———	———	———	———	———	———	———	———	———
BaO	———	———	———	———	< 0.01	———	———	———	———

those of the Quebec iron formation, the iron formation shows the greatest similarities to sidiritic and bog iron sediments and the greatest differences from oolitic-siliceous and lateritic types. An interesting comparison may also be made with analyses of iron-bearing carbonate rocks of the Lake Superior region tabulated by Irving and Van Hise (1892). These rocks, which probably are similar to the original unmetamorphosed Quebec iron formation, resemble the latter in great detail. This is especially true with respect to their low contents of TiO_2 and Al_2O_3 and their variable contents of CaO and MgO.

In table 2 two spectrographic analyses of Precambrian iron-bearing rocks from other areas are presented. Specimen KL is minnesotaite-quartz iron formation from the Labrador trough, and MM-2 is cummingtonite-quartz-magnetite iron formation from the Michigamme Mine of Michigan. The low concentrations of the minor oxides and the general level of concentration of Al_2O_3 and MnO also suggest kinship with the Quebec iron formation.

TABLE 2

Analyses of minerals and rocks

	DH-3	KL	MM-2	2G	4G	2B	9B
SiO_2	48.48	60.0	44.0	nd	nd	nd	nd
TiO_2	0.01	———	< 0.01	< 0.04	< 0.04	———	———
Al_2O_3	1.19	< 0.1	2.1	nd	nd	nd	nd
Fe		24.5	33.0	nd	nd	nd	nd
Fe_2O_3	2.40	nd	nd	nd	nd	nd	nd
FeO	42.05	nd	nd	nd	nd	nd	nd
MnO	2.80	0.14	1.05	< 0.02	< 0.02	< 0.02	0.035
MgO	1.93	3.0	4.0	nd	nd	nd	nd
CaO	0.00	0.10	0.48	nd	nd	nd	nd
Na_2O	0.12	nd	nd	nd	nd	nd	nd
K_2O	0.02	nd	nd	nd	nd	nd	nd
ZrO_2	nd	———	———	nd	nd	nd	nd
V_2O_3	nd	———	———	———	———	< 0.03	0.03
Cr_2O_3	nd	———	———	———	———	———	———
NiO	nd	———	———	———	———	———	———
SrO	nd	———	———	nd	nd	nd	nd
BaO	nd	———	———	nd	nd	nd	nd
H_2O^+	1.58	nd	nd	nd	nd	nd	nd
H_2O^-	0.00	nd	nd	nd	nd	nd	nd
F	0.00	nd	nd	nd	nd	nd	nd

Symbols are the same as in table 1.

DH-3 is a chemical analysis of cummingtonite from the Quebec iron formation (H. B. Wiik analyst). The exact location of this specimen is unknown. KL is minnesotaite-quartz rock from the Labrador trough (the writer is indebted to Mr. Edward J. Olsen for this specimen). MM-2 is cummingtonite-quartz-magnetite rock from the Michigamme Mine, Michigan. Specimens 2G and 4G are hematites which coexist with corresponding specimens of table 1. Specimens 2B and 9B are magnetites which coexist with corresponding specimens of table 1.

The bulk chemical characteristics of the Quebec iron formation and its previously-described structural features seem to imply that it was chemically

deposited as a siliceous carbonate sediment, although some of the iron may have been deposited as oxides or hydroxides. From the low aluminum content it appears that suspended matter was virtually excluded from the area of sedimentation. This is also indicated by the apparent lack of detectable quantities of zirconium.

It may be argued that metamorphic differentiation could have given rise to the chemical features of the Quebec iron formation. However, it would seem improbable that differentiation in this locality should develop rocks whose chemistry is so similar to common iron-bearing sediments.

The mineral assemblages.—The specimens have been divided, on the basis of the iron oxide phases, into two major groups designated A and B. These groups have been subdivided into the assemblages indicated by the numeral subscripts (table 4). Group A is characterized by the single iron oxide magnetite. Group B is characterized by hematite, although assemblages B_1, B_2, and B_3 contain magnetite as well. Assemblage B_4 is represented by only one specimen and is thought to contain hematite as the only coexisting oxide phase. However, in B_4 the coexistence of the oxides was difficult to assess due to small amounts of magnetite in the adjacent bands.

TABLE 3

Refractive indices of actinolites and dolomites from the iron formation

Rock	N_γ Actinolite	N_ω Dolomite	Rock	N_γ Actinolite	N_ω Dolomite
DH3-172	1.658		2G	1.627	
B-13	1.670		4G	1.627	1.686
DH10-158	1.649		8G	1.628	
DH7-484		1.705	Dr-1	1.626	
B-22	1.639		14G	1.627	
DH7-482		1.698	DHl-21	1.627	
B-20	1.647		DHl-32	1.628	1.688
DH7-445	1.643		DHl-52	1.627	
12BA	1.655		DH4-185	1.630	
12AB	1.655		DH7-480	1.627	1.686
DH10-101	1.634		DH11-200	1.628	1.688
9G	1.639		10G	1.628	
G-15	1.643		DH13-607	1.628	
DH10-85		1.710	DH7-291	1.623	
F-1	1.629				

The precision is approximately ± 0.003 for indices up to 1.700; above this it is approximately ± 0.005.

Within a group the assemblages are distinguished by the types and numbers of mineral phases they contain. Assemblages of six and seven minerals, which appear to have the greatest thermodynamic significance, are represented by A_1, B_1, B_2, and B_3 as follows:

A_1	B_1	B_2	B_3
cummingtonite	actinolite	cummingtonite	Ca-pyroxene
Ca-pyroxene	talc	actinolite	actinolite
actinolite	magnetite	talc	magnetite
magnetite	hematite	magnetite	hematite
calcite	calcite	hematite	calcite
quartz	dolomite	quartz	quartz
	quartz		

Assemblages A_2 and A_3 are in general incomplete versions of A_1 except that dolomite occurs in some specimens of A_2. Also some specimens of A_2 contain as many as six minerals. However, these minerals are different in different specimens or require the addition of components such as bismuth. Assemblage B_4 (actinolite-talc-hematite-dolomite-quartz) is an incomplete version of B_1. Assemblage A_5 (actinolite-talc-magnetite-quartz), although placed in the A group on the basis of the absence of hematite, may also be regarded as an incomplete version of B_1 or B_2. Assemblage A_4, which contains chlorite, will not be discussed further. Such minerals as chlorite, metallic bismuth, and pyrite require the addition of Al, Bi, and S to the seven major components to explain their existence. However, since these occurrences are minor and in any case involve an additional phase for each additional component, they do not affect conclusions based on the phase rule. Also Bi and S probably do not enter the silicates in more than trace amounts.

Wide variation of Fe and Mg in the ferromagnesian minerals is characteristic of the A group of assemblages which contain magnetite as the only oxide phase, whereas variations in the concentrations of the minor elements are shown by all of the assemblages. This variation makes it possible to plot the atomic ratios Mg/(Mg + Fe) and Mn/(Mg + fe + Mn) as shown in figures 2 through 8. These figures, with the exception of 8, are similar to the Roozeboom type curves for aqueous solutions in equilibrium with solid solutions. This type of plot for coexisting minerals was used by Kretz (1959) who has discovered many interesting facts through its utilization.

An idea of the maximum amount of scatter of points expected in figures 2 through 8 from the degree of precision of the analytical data may be gained by applying the following expression to the points:

$$\Delta x = 2p(x - x^2) \quad . \tag{1}$$

Here Δx is the maximum scatter in the atomic ratios as a function of the atomic ratio and the precision p in the weight determinations. Here p is assumed to have the constant value of $\pm$ 0.05 for Mg, Fe, and Mn over the entire range of x. This is of course not strictly true, but it is believed to be a good approximation for the range of compositions represented. This expression is derived by taking the differential of x, dx, which is then a function of the differentials of the weight percents of the different elements contained in x. These differentials are equal to the products of the weight percents and p. If the signs of the differentials of the weight percents in the expression for dx are then changed in such a manner as to make dx a maximum, the expression for Δx is the result. It is seen that this expression has a maximum of $\Delta x = \pm$ 0.025

TABLE 4

Mineral assemblages and atomic ratios of minerals from the Quebec iron formation

Assemblage	A_1				A_2			
Specimen No.	B-15	DH3-172	DH9-324	DH10-169	2B	B-13	B-16	DH3-149
Mg/(Mg + Fe)	0.197	0.332	0.270	0.259	0.115	0.217	0.169	0.280
Cummingtonite								
Mn/(Mg+Fe+Mn)	0.0150	0.0323	0.0369	0.0210	0.0146	0.0108	0.0146	0.0422
Mg/(Mg + Fe)	0.261	0.425	0.334	0.304	0.114	0.313	0.222	0.364
Ca-pyroxene								
Mn/(Mg+Fe+Mn)	0.0134	0.0292	0.0347	0.0208	0.0155	0.00785	0.0125	0.0399
Mg/(Mg + Fe)		0.440				0.286		
Actinolite	+		+	+	+		+	+
Mn/(Mg+Fe+Mn)		0.0198				0.00532		
Talc	—	—	—	—	—	—	—	—
Magnetite	+	+	+	+	+	+	+	+
Hematite	—	—	—	—	—	—	—	—
Calcite	Undif.	+	+	+	—	—	—	—
Mg/(Mg + Fe)	Carb.							
Dolomite		—	—	—	—	—	—	—
Quartz	+	+	+	+	—	+	+	+
Other	—	—	—	—	—	—	—	—

"—" indicates that the mineral was not observed. "+" indicates that the mineral was observed.
"Undif. Carb." indicates that the carbonate is undifferentiated and may consist of calcite and/or dolomite.
Mg/(Mg + Fe) for dolomite is approximate from refractive indices using the curve of Winchell (1951).

TABLE 4 (Continued)

Assemblage	A_2							
Specimen No.	CL-1	6B	B-14	DH5-77	DH10-131	DH10-158	B-19	DH7-484
Mg/(Mg + Fe) Cummingtonite	0.252	0.292	0.160	0.274	0.305	0.420	0.235	0.510
Mn/(Mg+Fe+Mn)	0.0160	0.0122	0.0143	0.0408	0.0320	0.0174	0.0129	0.0263
Mg/(Mg + Fe) Ca-pyroxene	0.342	0.324	0.218	0.360	—	—	—	—
Mn/(Mg+Fe+Mn)	0.0147	0.0109	0.0132	0.0407				
Mg/(Mg + Fe) Actinolite	+	—	—	—	+	0.573	+	+
Mn/(Mg+Fe+Mn)						0.00695		
Talc	—	—	—	—	—	—	—	—
Magnetite	+	+	+	+	+	+	+	+
Hematite	—	—	—	—	—	—	—	—
Calcite	—	+	+	—	Undif.	—	—	—
Mg/(Mg + Fe) Dolomite	—	—	—	—	Carb.	—	—	~0.70
Quartz	+	—	+	+	—	+	+	+
Other	—	—	—	—	—	—	pyrite	metallic bismuth

TABLE 4 (Continued)

Assemblage	A_2							
Specimen No.	DH10-95	B-22	B-22A	DH10-78	DH7-482	7B	B-20	3B
Mg/(Mg + Fe)	0.539	0.543	0.369	0.498	0.622	0.354	—	—
Cummingtonite								
Mn/(Mg+Fe+Mn)	0.0316	0.0112	0.00926	0.0194	0.0251	0.0104		
Mg/(Mg + Fe)							0.581	0.480
Ca-pyroxene	—	—	—	—	—	—		
Mn/(Mg+Fe+Mn)							0.00934	0.0105
Mg/(Mg + Fe)		0.693					0.608	
Actinolite	+		—	—	—	—		+
Mn/(Mg+Fe+Mn)		0.00675					0.00638	
Talc	—	—	—	—	—	—	—	—
Magnetite	+	+	+	+	+	+	+	+
Hematite	—	—	—	—	—	—	—	—
Calcite	+	+	+	+	—	+	—	+
Mg/(Mg + Fe)					~0.75			
Dolomite	+	—	—	+		—	—	—
Quartz	+	+	+	+	+	—	+	+
Other	—	—	—	—	—	—	—	—

TABLE 4 (Continued)

Assemblage	A_2						A_3	
Specimen No.	DH7-445	12BA	12AB	DH10-101	9G	G-15	1B	8B
Mg/(Mg + Fe) Cummingtonite	—	—	—	—	—	—	0.0197	0.0248
Mn/(Mg+Fe+Mn)							0.0121	0.0264
Mg/(Mg + Fe) Ca-pyroxene	0.650	0.485	—	—	—	—	—	—
Mn/(Mg+Fe+Mn)	0.0237	0.0160						
Mg/(Mg + Fe) Actinolite	0.653	0.521	0.506	0.795	0.721	0.661		
Mn/(Mg+Fe+Mn)	0.0172	0.00774	0.00918	0.0135	0.0139	0.0188	—	—
Talc	—	—	—	—	—	—	—	—
Magnetite	+	+	+	+	+	+	+	+
Hematite	—	—	—	—	—	—	—	—
Calcite	Undif. Carb.	+	Undif. Carb.	—	—	—	—	—
Mg/(Mg + Fe) Dolomite		—		—	—	—	—	—
Quartz	+	+	+	+	+	+	+	+
Other	—	metallic bismuth	metallic bismuth	—	—	—	—	—

TABLE 4 (Continued)

Assemblage	A_3		A_4		A_6	B_1		
Specimen No.	9B	B-17	DH7-490	DH10-85	F-1	2G	4G	8G
Mg/(Mg + Fe) Cummingtonite	0.0517	0.0854	0.483	0.431	—	—	—	—
Mn/(Mg + Fe + Mn)	0.0226	0.0164	0.0277	0.0286				
Mg/(Mg + Fe) Ca-pyroxene	—	—	—	—	—	—	—	—
Mn/(Mg + Fe + Mn)					0.827	0.867	0.864	0.871
Mg/(Mg + Fe) Actinolite	—	—	—	—				
Mn/(Mg + Fe + Mn)					0.00234	0.0130	0.00535	0.00671
Talc	—	—	—	—	+	—	+	+
Magnetite	+	+	+	+	+	+	+	+
Hematite	—	—	—	—	—	+	+	+
Calcite	—	—	Undif.	—	—	+	—	Undif.
Mg/(Mg + Fe)			Carb.	~0.65			~0.90	Carb.
Dolomite	—	—			—	—		
Quartz	+	+	+	+	+	+	+	+
Other	—	—	chlorite	chlorite	—	—	—	—

TABLE 4 (Continued)

Assemblage	B_1							
Specimen No.	Dr-1	14G	DH1-21	DH1-32	DH1-52	DH4-185	DH7-480	DH11-200
Mg/(Mg+Fe) Cummingtonite	—	—	—	—	—	—	—	—
Mn/(Mg+Fe+Mn) Mg/(Mg+Fe) Ca-pyroxene	—	—	—	—	—	—	—	—
Mn/(Mg+Fe+Mn) Mg/(Mg+Fe) Actinolite	0.880	0.870	0.872	0.864	0.871	0.844	0.854	0.877
Mn/(Mg+Fe+Mn)	0.00903	0.0100	0.00632	0.00674	0.00568	0.0112	0.00984	0.00852
Talc	+	+	+	+	+	+	+	+
Magnetite	+	+	+	+	+	+	+	+
Hematite	+	+	+	+	+	+	+	+
Calcite	—	+	Undif.	—	+	+	+	+
Mg/(Mg+Fe) Dolomite	+	—	Carb.	~0.90	+	+	~0.90	~0.90
Quartz	+	+	+	+	+	+	+	+
Other	—	—	—	—	—	—	—	—

TABLE 4 (Continued)

Assemblage	B_2	B_3	B_4
Specimen No.	10G	DH13–607	DH7–291
Mg/(Mg+Fe) Cummingtonite	0.770	—	—
Mn/(Mg+Fe+Mn) Mg/(Mg+Fe) Ca-pyroxene	0.0150 —	0.841	—
Mn/(Mg+Fe+Mn) Mg/(Mg+Fe) Actinolite	0.871	0.0164 0.862	0.908
Mn/(Mg+Fe+Mn)	0.00558	0.0111	0.00870
Talc	+	—	+
Magnetite	+	+	—
Hematite	+	+	+
Calcite Mg/(Mg+Fe) Dolomite	—	+ —	— +
Quartz	+	+	+
Other	—	—	—

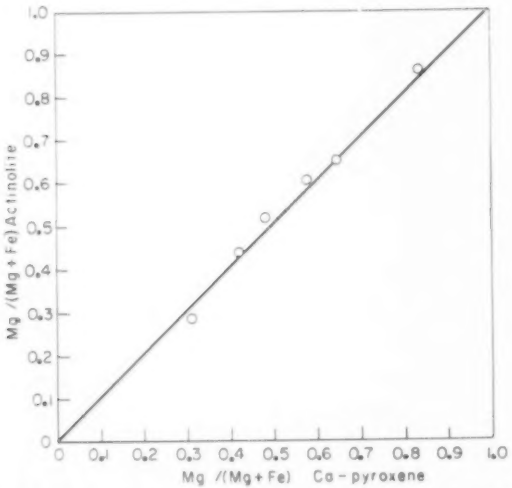

Fig. 2. Relation between the atomic ratios of magnesium in coexisting Ca-pyroxene and actinolites from the Quebec iron formation. The curve is arbitrarily drawn at 45°. The mineral pairs represented all coexist with magnetite. The pair represented by the point at far right coexists with magnetite and hematite.

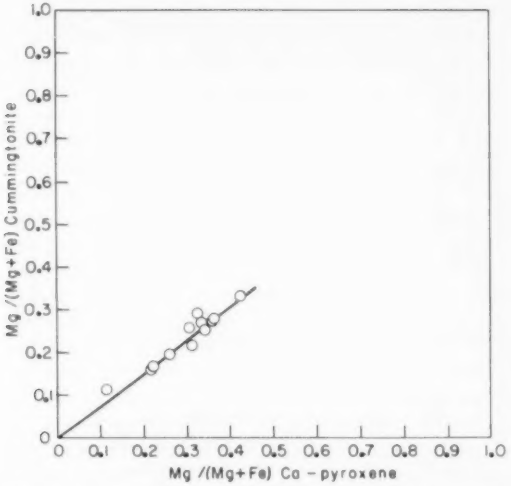

Fig. 3. Relation between the atomic ratios of magnesium in coexisting Ca-pyroxenes and cummingtonites from the Quebec iron formation. The mineral pairs represented all coexist with magnetite as the only iron oxide phase.

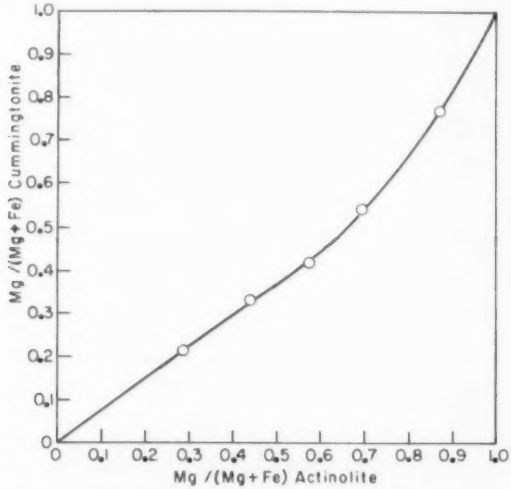

Fig. 4. Relation between the atomic ratios of magnesium in coexisting actinolites and cummingtonites from the Quebec iron formation. The mineral pairs represented all coexist with magnetite. The pair represented by the point on the far right coexists with magnetite and hematite.

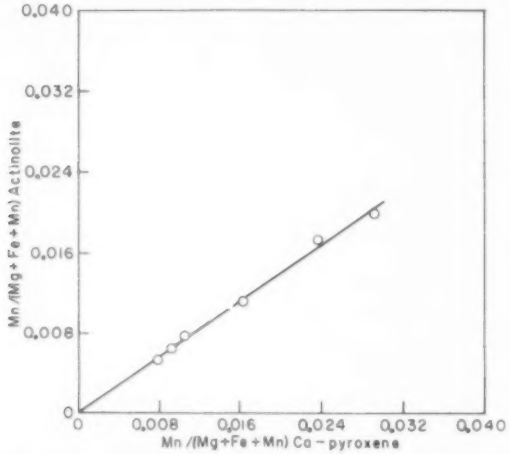

Fig. 5. Relation between the atomic ratios of manganese in coexisting Ca-pyroxenes and actinolites from the Quebec iron formation.

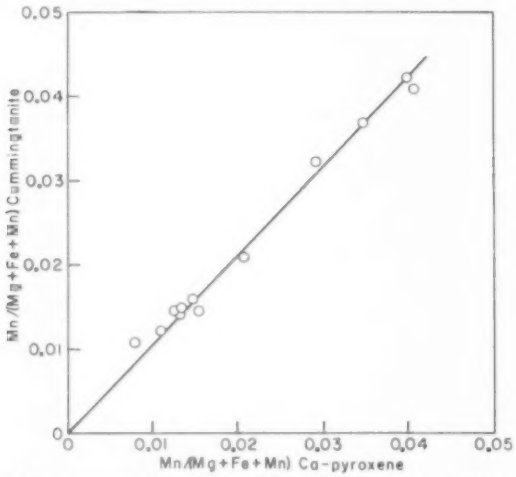

Fig. 6. Relation between the atomic ratios of manganese in coexisting Ca-pyroxenes and cummingtonites from the Quebec iron formation.

at $x = 0.5$ and decreases to zero at $x = 1$.

Figures 2, 3, and 4 show that Mg and Fe are almost equally distributed between actinolite and Ca-pyroxene, but that these minerals take notably more Mg than the coexisting cummingtonite. The precise forms of the curves over the whole range are uncertain because of insufficient data and scatter. However, figure 2 appears to be nearly linear within the range of expected scatter.

whereas figures 3 and 4 seem to approach linearity in the region Mg/(Mg + Fe) = 0 to 0.5. Note that the curve of figure 4 seems to be asymmetrical with greater curvature toward the Mg end. This feature, to be discussed later, is probably of some importance as an indication of the character of the solid solutions. Also, because of the nearly equal distribution of Mg and Fe between actinolite and Ca-pyroxene, the distribution curves of figures 3 and 4 are near duplicates over the observed range. Another important feature of figures 2 and 4 is that the most Mg-rich mineral pairs of these figures, representing assemblages B_2 and B_3, coexist with hematite in addition to magnetite. The other pairs, which show great variation in Mg/(Mg + Fe), are all from the A group of assemblages and coexist with magnetite as the only iron oxide phase.

The distribution of Mn is shown in figures 5, 6, and 7. Curves 5 and 6 show close approach to linearity. Because of the scatter of points shown by figure 7, the curve for the figure has been calculated from the slopes (assumed to be constant) of figures 5 and 6. Since this calculation involves the errors of both of these curves, the curve of figure 7 passes to the right of most of the points. Three mineral pairs of figure 7 do not occur in figures 5 and 6, and two of these pairs show a scatter which is considerably greater than that expected from equation (1).

All the curves except figure 7 show a scatter of points which is nearly always within the maximum attributable to the analytic precision. In anticipation of the following discussion, this may be interpreted as a close approach to chemical equilibrium. In this context the scatter in figure 7 (if not due to large errors) may be the result of the failure of Mn to attain equilibrium throughout the volume occupied by the minerals analyzed.

The general chemical and physical characteristics of the ferromagnesian minerals suggest that most of their iron is in the ferrous state. Ferrous iron was determined for two iron formation silicates (tables 1 and 2). The results indicate a high ratio of ferrous to ferric iron.

As an additional check on the oxidation state of the iron in the actinolites, refractive indices were determined (table 3 and fig. 8). The curve of figure 8 indicates that the actinolites belong to the tremolite-ferrotremolite series as discussed by Foslie (1945).

Figure 8 also shows the correlation of the coexisting oxide phases with the Fe content of the actinolites. Great variation is shown by the actinolites of the A group of assemblages; but in the B group the compositions of all actinolites lie well toward the Mg end of the range. This effect is similar to that shown by figures 2 and 4.

Another interesting feature of figure 8 is the apparent restriction on the range of the Fe content in the actinolites of the B group assemblages. This range is little more than the maximum scatter expected from the analytical precision. Since B_2 and B_3 are represented by only one specimen each, it cannot be assumed that the iron contents of their actinolites is fixed as it appears to be for those of B_1. However, it is interesting that Fe/(Fe + Mg) of actinolite in these three assemblages is nearly the same. In the next section it will be demonstrated that this result is to be expected if chemical equilibrium and uniform P-T conditions prevailed in all three assemblages. It will also be demon-

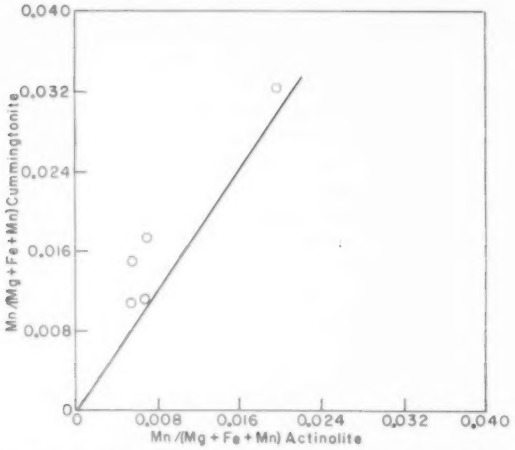

Fig. 7. Relation between the atomic ratios of manganese in coexisting actinolites and cummingtonites from the Quebec iron formation. The slope of the line was calculated from the slopes of figures 5 and 6 and shows the expected relation.

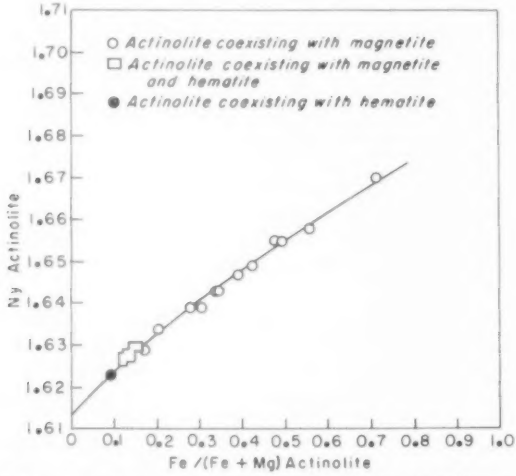

Fig. 8. Refractive indices of twenty-six iron formation actinolites as related to the atomic ratio. The curve has been extrapolated to the index of pure tremolite.

strated that the association of magnesium-rich ferromagnesian silicates with hematite is a consequence of these same equilibrium conditions.

The iron contents of some dolomites from the assemblages were determined optically (tables 3 and 4) using the curve of Winchell (1951). The results have not been plotted; however, the values obtained seem to indicate

that the Fe contents of dolomite and the coexisting silicates are related to each other.

A specimen of talc from assemblage B_1 was analyzed. The talc could not be obtained in pure form due to inclusions of other minerals. The observed constituents are as follows: $SiO_2 - 73.0$, $Al_2O_3 - 0.3$, $Fe - 1.90$, $MnO - 0.24$, $MgO - 18.0$, $CaO - 0.3$. No other oxides were detected. $N_z = 1.590$. Most of the iron and some of the silica is probably attributable to inclusions.

A comparison of some of the compositional features of the four critical assemblages A_1, B_1, B_2, and B_3 is presented in figure 9. This tetrahedron shows the relations of the silicate solid solution series to the iron oxide phases. Other phases are not shown. Since the system treated is really one of seven components, this figure cannot show all the possible assemblages even under isothermal and isobaric conditions and thus differs from equilibrium diagrams conventionally used to represent four component systems. In figure 9 the choice of components is necesarily arbitrary and was made in such a way as to give what appears to be the simplest picture of the system. Assemblages B_3 and B_2 are represented by the two small distorted tetrahedra, the corners of which are indicated by unprimed mineral symbols. The common face of these two tetrahedra represents assemblage B_1, which is represented by a plane rather than

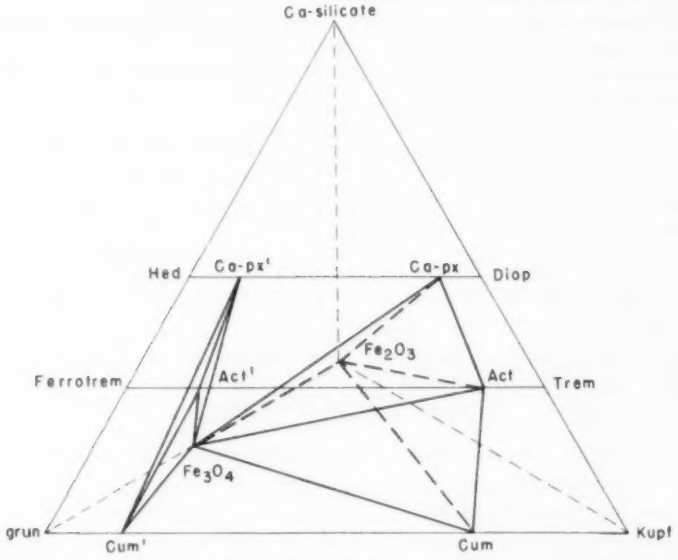

9. Tetrahedron showing the compositional relations of assemblages A_1, B_1, B_2, and B_3. Mineral symbols are as follows: Kupf = kupfferite, grun = grunerite, Trem = tremolite, Ferrotrem = ferrotremolite, Diop = diopside, Hed = hedenbergite, Cum = cummingtonite, Act = actinolite, and Ca-px = Ca-pyroxene. The small distorted tetrahedra (heavy lines) and their faces represent the mineral assemblages as follows: A_1, tetrahedron Cum′–Ca-px′–Act′–Fe_3O_4; B_1, plane Act–Fe_3O_4–Fe_2O_3; B_2, tetrahedron Cum–Act–Fe_3O_4–Fe_2O_3; B, tetrahedron Ca-px–Act–Fe_3O_4–Fe_2O_3.

by a tetrahedron because it contains only one silicate solid solution. It is interesting to compare these three assemblages in terms of the minerals not shown in figure 9. Thus B_3 which lies in a region of figure 9 in which (Mg + Fe)/Ca is small contains as an additional phase calcite in which this ratio is also small. Similarly assemblage B_1 which lies in a region in which (Mg + Fe)/Ca is intermediated contains the additional minerals calcite, dolomite and talc in which (Mg + Fe)/Ca shows a wide range. Finally assemblage B_2 contains, with the exception of quartz, only the additional phase talc in which (Mg + Fe)/Ca is large, which also corresponds to the position of this assemblage in figure 9. From these relationships it appears that figure 9, although only a partial representation of the assemblages, reflects the complete assemblages, in terms of Ca, Mg, and Fe contents of the rocks.

The corner "Act" of figure 9 is a unique point inasmuch as it represents the constant (uniform) Mg/(Mg + Fe) ratio of the actinolites of assemblages B_1, B_2, and B_3 which was discussed previously with reference to figure 8.

Assemblage A_1 is represented by the small distorted tetrahedron with primed mineral symbols. This tetrahedron is however different from the tetrahedra with the corner "Act" insomuch as its position may vary in terms of Mg/Fe ratios depending on factors impossible to show in figure 9. As will be indicated in the following discussion one of these factors may be the partial pressure of oxygen. Thus there are an infinite number of possible tetrahedra representing assemblage A_1. Various positions of some of these tetrahedra may be constructed from the data of table 4. However their total range in figure 9 is not known.

The effect of variation of bulk composition on the ferromagnesian minerals is also illustrated by assemblage A_3 (table 4) in which the rocks approach the system FeO–O–SiO_2–H_2O. The other major components in this case assume roles of minor constituents with manganese and other elements in low concentration.

THEORETICAL INTERPRETATION OF THE MINERAL ASSEMBLAGES

Symbols and assumptions.—The following symbols and assumptions are used in the discussion except where otherwise stated.

$X_{or\text{-}px}$	atomic ratio $Mg/(Mg + Fe^{2+})$ in orthopyroxene
$X_{Ca\text{-}px}$	atomic ratio $Mg/(Mg + Fe^{2+})$ in Ca-pyroxene
X_{act}	atomic ratio $Mg/(Mg + Fe^{2+})$ in actinolite
X_{cum}	atomic ratio $Mg/(Mg + Fe^{2+})$ in cummingtonite
R	gas constant
T	absolute temperature
P	pressure
G	Gibbs free energy

The superscript "o" refers to substances at one atmosphere pressure and at any temperature. Small letter subscripts refer to the chemical reactions. Various pressures are distinguished by subscripts which indicate the substances to which they refer.

The assumptions are as follows: The solid solution series are treated as ideal solutions of the hypothetical mineral end members, as for example, $CaMgSi_2O_6$ (diopside) and $CaFeSi_2O_6$ (hedenbergite). Mg and Fe^{2+} under these conditions must be regarded as completely disordered with respect to each other. Any ordering in a real crystal would then manifest itself as a deviation from the ideal solution. Also quartz, calcite, hematite, magnetite, and talc are regarded as compounds of fixed composition. The compressibilities and thermal expansions of minerals are disregarded.

The Quebec iron formation is regarded as belonging to that class of systems exhibiting critical phenomena. According to Fyfe, Turner, and Verhoogen (1958), almost all mineral systems with the exception of those containing halides and alkali-metal silicates, fall into this class. The above assumption thus seems warranted, at least as a first approximation, for a system composed of the seven major components of the iron formation. The possible occurrence at the time of crystallization of significant quantities of halogens and alkalies in the dispersed fluid phase of the iron formation is disregarded, although it cannot be discounted as a possibility. In view of these postulated properties of the system and the general mineralogy of the iron formation, which indicates the amphibolite facies, it is supposed that the rocks crystallized above the critical temperature of water. The fluid is then treated as a gaseous mixture. As an additional simplification these gases are regarded as perfect, an approximation which is valid only at low pressures. However, the partial pressures as written in the theoretical functions are, in any case, really fugacities, and may be regarded as such at any pressure without detraction from the argument.

Equilibrium between Ca-pyroxene and orthopyroxene.—In order to elucidate the iron formation assemblages it is interesting to consider the equilibrium between Ca-pyroxene and orthopyroxene. These minerals seem to provide an informative illustration of the basis for the distribution of elements among coexisting minerals.

If two minerals form ideal solid solutions involving two ions such as Mg and Fe^{2+}, it is possible to represent the distribution equilibrium by a simple ion exchange reaction and the concentrations expressed as atomic ratios. The equations have been discussed by Ramberg and Devore (1951) and by Ramberg (1952). Analogous experimental systems involving coexisting aqueous and solid solutions have been treated by Hill, Durham, and Ricci (1940).

The exchange reaction in the case of Ca-pyroxene and orthopyroxene is

$$\underset{\text{diopside}}{CaMgSi_2O_6} + \underset{\text{ferrosilite}}{FeSiO_3} \rightarrow \underset{\text{hedenbergite}}{CaFeSi_2O_6} + \underset{\text{enstatite}}{MgSiO_3} \qquad \text{(a)}$$

Let the change in Gibbs free energy for this reaction between the pure end members be called ΔG°. Then the total change in Gibbs free energy when one mole of Mg in Ca-pyroxene of the equilibrium composition $X_{Ca\text{-}px}$ is exchanged for one mole of Fe^{2+} in orthopyroxene of the equilibrium composition $X_{or\text{-}px}$ is

$$\Delta G_a = 0 = \Delta G_a^\circ - RT\ln \frac{X_{Ca\text{-}px}(1 - X_{or\text{-}px})}{X_{or\text{-}px}(1 - X_{Ca\text{-}px})} . \qquad (2)$$

At constant temperature

$$\exp \frac{\Delta G_a^\circ}{RT} = K_a ,$$

where K_a is the equilibrium (distribution) constant.
Consequently,

$$X_{or\text{-}px} = \frac{X_{Ca\text{-}px}}{K_a + X_{Ca\text{-}px} - K_a X_{Ca\text{-}px}} . \qquad (3)$$

Since the reaction involves only solids, it should be relatively insensitive to pressure. Thus if K_a were temperature-sensitive enough, and were known as a function of temperature, the observed equilibrium distribution might be used to obtain the temperature of crystallization. Unfortunately, the necessary thermal data do not yet exist for this reaction.

However, equation (3) provides a test for the degree of ideality of the solid solutions if the compositions of a series of coexisting minerals which crystallized under the same P-T conditions are known. Howie (1955) gives compositions for six pairs of coexisting Ca-pyroxenes and orthopyroxenes from the charnockites of Madras, India, which presumably approximate this requirement. Values of $Mg/(Mg + Fe^{2+})$ for these pairs are given in table 5. These values have been plotted in figure 10 and the theoretical curve with $K_a = 1.82$ superimposed. From the degree of correspondence, it seems that the assumption of ideal solutions is justified for this range of compositions. This seems to substantiate the conclusions of Sahama and Torgeson (1949) with respect to orthopyroxene.

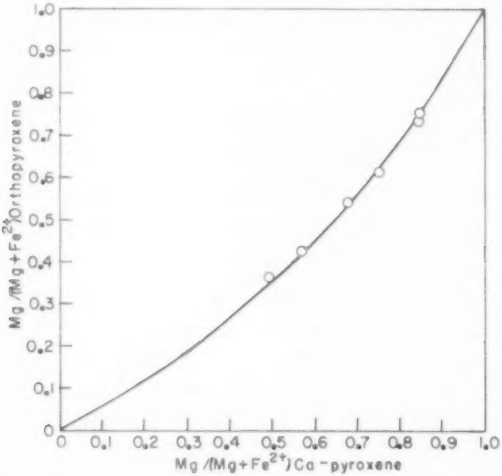

Fig. 10. Relation between the atomic ratios of magnesium in coexisting Ca-pyroxenes and orthopyroxenes from the Charnockite series of Madras, India. Data taken from Howie (1955). The curve is theoretical assuming ideal solid solutions.

Distribution curves such as figure 10 reflect equilibrium adjustments of coexisting minerals to variations in bulk composition in those systems which retain at least one degree of freedom under uniform (constant) P-T conditions. The solid solutions may not always be ideal as they appear to be in this case. Varying degrees of non-ideality may cause the curves to assume different forms. Also, variations in the concentrations of other elements may cause apparent erratic scatter of points with consequent dissolution of the curve, as has been observed by Kretz (1959). That such erratic distributions are only apparent in some cases was demonstrated by Kretz in an elegant manner by relating the concentrations of certain extraneous elements to the amount and direction of scattering. This effect is highly specific for different elements and minerals and indicates in itself a strong tendency toward equilibrium.

The distribution constants (or functions in case of non-ideality) are unaffected by the presence of other phases if the bulk composition changes accompanying the appearance or disappearance of these phases are not correlated with changes in concentration of extraneous elements in the phases under consideration. Even when pairs of minerals show variations in other elements the effect may be small if the variations are within certain bounds. Thus the pairs utilized in figure 10 show variations in Al_2O_3, Fe_2O_3, TiO_2, and other components (Howie, 1955), but this variation appears to introduce little scatter.

Distribution of Mg, Fe, and Mn among coexisting minerals of the iron formation.—It is apparent from figures 2 through 7 that there are systematic chemical relations between coexisting minerals of the iron formation which resemble those just discussed. In the iron formation extraneous ions which might affect the distributions of Mg, Fe, and Mn appear to be in low concentrations. Also since the preponderant part of the iron in the ferromagnesian minerals is probably in the ferrous state, the free mutual substitution of Mg and Fe is favored. Indeed, there appears to be no obvious interaction between Mg, Fe, and Mn except for the reciprocal effect of mutual replacement. In the case of Mn, the concentration range is not great enough to reveal with certainty which

TABLE 5

Atomic ratios of coexisting orthopyroxenes and Ca-pyroxenes from the charnockite series of Madras, India
(Data from Howie, 1955)

	$Mg/(Mg + Fe^{++})$	
Specimen	Orthopyroxene	Ca-pyroxene
3709	0.756	0.848
4645	0.735	0.846
2270	0.616	0.751
2941	0.543	0.678
4642A	0.429	0.570
115	0.368	0.492

elements are replaced. However, the systematic variation of the ratio Mn/(Mg + Fe + Mn) leads one to suspect that Mn replaces Mg and Fe^{2+}.

In figure 2 the distribution function is close to the constant value of one, as may be seen from the straight line which has been drawn for comparison. This straight line represents a special case of a family of curves similar to that of figure 10. All of the curves, including the straight line, represent distributions for coexisting ideal solutions. Therefore figure 2 seems to indicate a close approach to ideal solid solutions for actinolite and Ca-pyroxene. In the case of Ca-pyroxene this conclusion agrees with the interpretation of figure 10. Figures 3 and 4 show linearity to approximately Mg/(Mg + Fe) = 0.5 and their slopes are the same within the precision of the analytical data. As was previously mentioned, the equality of the slopes of figures 3 and 4 is a consequence of the slope of figure 2, and either of these slopes might be calculated from the other two. Since curves 3 and 4 appear to be linear over much of their range but do not have slopes equal to unity, they cannot represent ideal solutions. This non-ideal behavior can only be attributed to cummingtonite.

Each of the curves of figures 2, 3, and 4 are in part based upon data not contained in the other two curves. Furthermore the mineral pairs represented by different points of the same figure frequently do not occur in identical assemblages (table 4). These features illustrate the fact that the distribution functions are independent of the mere presence or absence of other phases.

In the examples of the distribution of Mn (figs. 5, 6, and 7), the degree of correspondence to ideal solutions is indeterminate because of the limited range of compositions. However, curves 5 and 6 appear to be nearly linear as might be expected from the Nernst distribution law for dilute solutions.

General equilibrium relations in the B-group assemblages disregarding differences in volume between solid reactants and products.—If the minor elements are disregarded it is possible to treat the iron formation as a system of the seven major components CaO, MgO, FeO, O, SiO_2, H_2O, and CO_2. These components then enter into coupled chemical reactions which include every mineral of the rock and the postulated gaseous phase. All possible reactions between phases actually present must be given equal consideration in the sense that at equilibrium the total change in free energy for each reaction must be zero. The reactions then yield equilibrium constants of various types among which are the distribution constants.

The device of disregarding, as a first approximation at this time, the differences in volume between the solid reactants and products has as its object the simplification of the theoretical equations, since the consideration of these volume changes would require, in addition to the variable of total gas pressure, the simultaneous consideration of a variable corresponding to the rock pressure acting on the solid phases. The two pressures in general are probably not the same. Disregarding the solid phase volume changes makes it possible to drop the rock pressure variable. Apart from considerations of simplicity this is, as will be shown, also justified by the relatively close proximities of the specimens studied. Thus the rock pressure may be considered as a constant. Under these circumstances the phase rule takes the form $v = (c + 2) - p$, where v is the variance, c the number of components and p the number of phases. The

figure 2 represents the temperature and total gas pressure variables. In this system the total gas pressure would be expected to correspond essentially to $P_{H_2O} + P_{CO_2}$, and would appear to have as its upper limit the rock pressure.

The coupled reactions in assemblage B_1 will be considered first. In this assemblage there are generally seven mineral phases; and in addition to these a gas phase is assumed to be present. The chemical content of the system requires the consideration of certain possible oxidation reactions. Two of these reactions involve the oxidation of H_2 and CO to H_2O and CO_2 and give rise to the equilibrium concentrations of these gases. Since both magnetite and hematite are present, there are also four possible reactions which involve the oxidation of ferrous iron in the actinolite and the dolomite to magnetite and hematite. Finally, there is the oxidation of magnetite to hematite. These reactions are not all independent since the oxidation of the ferrous components of the ferromagnesian minerals to magnetite and hematite is really equivalent to the simple oxidation of magnetite to hematite. Thus if magnetite and hematite are stoichiometric compounds the partial pressure of oxygen is a function of the temperature only. The same reasoning holds for assemblages B_2 and B_3 and makes it possible, under uniform temperature conditions, to omit further consideration of oxidation in comparing the three assemblages. However, several of the oxidation reactions mentioned here will be discussed in greater detail later when the A and B groups of assemblages are compared.

The following are non-oxidative reactions to be considered in assemblage B_1:

$$\underset{\text{tremolite}}{1/5\ Ca_2Mg_5Si_8O_{22}(OH)_2} + 2/15\ H_2O + 2/5\ CO_2 \rightarrow \underset{\text{talc}}{1/3\ Mg_3Si_4O_{10}(OH)_2} + 2/5\ \underset{\text{calcite}}{CaCO_3} + 4/15\ \underset{\text{quartz}}{SiO_2}\ , \qquad (b)$$

$$\underset{\text{ferrotremolite}}{1/5\ Ca_2Fe_5Si_8O_{22}(OH)_2} + 2/5\ CO_2 + \underset{\text{hematite}}{Fe_2O_3} \rightarrow 2/5\ \underset{\text{calcite}}{CaCO_3} + 8/5\ \underset{\text{quartz}}{SiO_2} + \underset{\text{magnetite}}{Fe_3O_4} + 1/5\ H_2O\ , \qquad (c)$$

$$\underset{\text{dolomite}}{CaMgC_2O_6} + 8/5\ \underset{\text{quartz}}{SiO_2} + 1/5\ H_2O \rightarrow \underset{\text{tremolite}}{1/5\ Ca_2Mg_5Si_8O_{22}(OH)_2} + 3/5\ \underset{\text{calcite}}{CaCO_3} + 7/5\ CO_2\ , \qquad (d)$$

$$\underset{\text{ferrodolomite}}{CaFeC_2O_6} + 8/5\ \underset{\text{quartz}}{SiO_2} + 1/5\ H_2O \rightarrow \underset{\text{ferrotremolite}}{1/5\ Ca_2Fe_5Si_8O_{22}(OH)_2} + 3/5\ \underset{\text{calcite}}{CaCO_3} + 7/5\ CO_2\ , \qquad (e)$$

$$\underset{\text{dolomite}}{CaMgC_2O_6} + 4/3\ \underset{\text{quartz}}{SiO_2} + 1/3\ H_2O \rightarrow \underset{\text{talc}}{1/3\ Mg_3Si_4O_{10}(OH)_2} + \underset{\text{calcite}}{CaCO_3} + CO_2\ , \qquad (f)$$

$$\underset{\text{ferrodolomite}}{CaFeC_2O_6} + \underset{\text{hematite}}{Fe_2O_3} \rightarrow \underset{\text{calcite}}{CaCO_3} + \underset{\text{magnetite}}{Fe_3O_4} + CO_2 \quad . \tag{g}$$

These reactions are all written for one mole of Mg and Fe^{2+} since the entropy of mixing which enters into the corresponding equations refers to the mixing of individual ions.

If dolomite is absent, only reactions (b) and (c) apply; and the equilibrium equations, taking into account the entropy of mixing of the ions and the gas pressures, are

$$\Delta G_b = 0 = \Delta G_b^\circ - RT\ln X_{act} + RT\ln \frac{1}{P_{co_2}^{2/5} P_{H_2O}^{2/15}} \tag{3}$$

and

$$\Delta G_c = 0 = \Delta G_c^\circ - RT\ln (1 - X_{act}) + RT\ln \frac{P_{H_2O}^{1/5}}{P_{co_2}^{2/5}} \quad . \tag{4}$$

At constant temperature the equivalent exponential forms are

$$\frac{K_b}{P_{co_2}^{2/5} P_{H_2O}^{2/15}} = X_{act} \tag{5}$$

and

$$\frac{K_c P_{H_2O}^{1/5}}{P_{co_2}^{2/5}} = 1 - X_{act} \quad . \tag{6}$$

where $K_b = \exp(\Delta G_b^\circ/RT)$ and $K_c = \exp(\Delta G_c^\circ/RT)$ are the equilibrium constants.

Therefore

$$P_{H_2O} = \left(\frac{K_b}{K_c}\right)^3 \left(\frac{1 - X_{act}}{X_{act}}\right)^3 \quad , \tag{7}$$

and

$$P_{co_2} = \frac{K_b^{3/2} K_c}{(1 - X_{act}) X_{act}^{3/2}} \quad . \tag{8}$$

Also by Dalton's law:

$$P = P_{H_2O} + P_{co_2} \quad . \tag{9}$$

Equation (9) is only an approximation at high pressures, but since the absolute values of the pressures are not known anyway it serves the purpose of illustration.

Figure 11 shows the graphs of P_{co_2}, P_{H_2O}, and P as functions of $Mg/(Mg + Fe^{2+})$ of actinolite in dolomite-free assemblage B_1. Since not all the thermal properties necessary to calculate K_b and K_c are known, it is necessary to assign some arbitrary values to these constants for plotting purposes. Therefore they have both been set equal to one, corresponding to $\Delta G_b^\circ = \Delta G_c^\circ = 0$. The

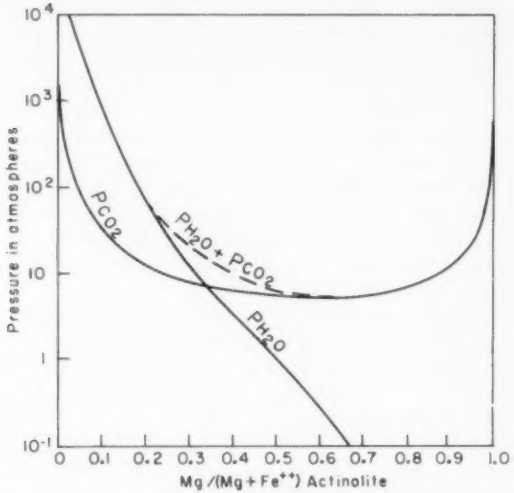

Fig. 11. Theoretical relation between the atomic ratio of magnesium in actinolite of dolomite-free assemblage B_1 and gas pressures. Perfect gases and ideal solid solution are assumed. Volume differences between solid reactants and products are disregarded, and all minerals except actinolite are assumed to be stoichiometric. The plot is for an arbitrary temperature at which $\Delta Gb^\circ = \Delta Gc^\circ = 0$. The forms and positions of the curves change with the temperature, but the general relations remain the same.

forms and positions of the curves of figure 11 would shift with changes in temperature, but the general relations would remain the same. Differentiation gives a minimum for P_{co_2} at $X_{act} = 0.6$, which holds for any temperature. The corresponding minimum of P is a function of the temperature but will always lie to the right of $X_{act} = 0.6$, as may be shown by considering the derivative of equation (9):

$$\frac{dp}{dX_{act}} = \frac{dP_{H_2O}}{dX_{act}} + \frac{dP_{CO_2}}{dX_{act}} \quad .$$

Since P_{H_2O} is a continuously decreasing function, the first term on the right is always negative, whereas for $X_{act} < 0.6$ the second term on the right is negative. This limits the minimum of P to the region $0.6 < X_{act} < 1$ at any temperature. It is interesting that the observed values of Mg/(Mg + Fe) of the actinolites from assemblages B_1, B_2, and B_3 fall within this range of possible minima. This fact may be of some consequence in that it might indicate that the assemblage formed at a gas pressure minimum.

In the region of Fe-rich actinolites P corresponds essentially to P_{H_2O}. In the region of Mg-rich actinolites, P corresponds to P_{CO_2}. Thus from the viewpoint of these rather simple and approximate equations Fe-rich actinolites of this assemblage appear to require relatively high gas pressures over a considerable range of compositions as compared with Mg-rich actinolites. The pressure of CO_2 is really immaterial to the stability of actinolite in the sense that this

mineral may be stable in the absence of CO_2. The CO_2 curve expresses the equilibrium pressure for calcite in association with actinolites of different compositions. If CO_2 is removed from the system, calcite disappears, and the system has the same number of degrees of freedom as before. The curve for P_{H_2O} in this case remains the same.

If dolomite is the only solid carbonate phase present, the composition of actinolite is still the same function of P_{H_2O}. However, P_{CO_2} is now a different function than that given by equation (8). The equation for P_{CO_2} in assemblage B_1 which contains only dolomite has not been derived because it is not known how closely dolomite approximates an ideal solution. However if the dolomite solutions were ideal, P_{CO_2} would be a linear function of $Mg/(Mg + Fe^{2+})$, as may be seen from reaction (g).

When both calcite and dolomite are present in assemblage B_1 (the commonest observed case), the system is univariant according to the phase rule. Then the compositions of all the minerals as well as the partial pressures of all the gases are determined at each temperature. This may also be understood by considering the two different expressions for P_{CO_2} involving calcite and dolomite, which must both be satisfied simultaneously. Therefore, if the temperature was uniform throughout the region where these rocks are found, the compositions of the minerals should also be uniform throughout this region. The observed uniformity is therefore consistent with phase rule considerations under uniform temperature conditions. This uniformity also seems to bear out the validity of the simplifying assumptions with respect to the effects of minor elements and the volume differences between solid reactants and products. It should also be noted that these phase rule considerations are independent of the nature of the chemical reactions as written. These equations may be regarded as simplifications which elucidate the real situation.

In assemblage B_2 the following non-oxidative reactions will be considered:

$$\underset{\text{kupfferite}}{1/7\ Mg_7Si_8O_{22}(OH)_2} + \underset{\text{quartz}}{4/21\ SiO_2} + 4/21\ H_2O \rightarrow \underset{\text{talc}}{1/3\ Mg_3Si_4O_{10}(OH)_2}\ . \tag{h}$$

$$\underset{\text{grunerite}}{1/7\ Fe_7Si_8O_{22}(OH)_2} + \underset{\text{hematite}}{Fe_2O_3} \rightarrow \underset{\text{magnetite}}{Fe_3O_4} + \underset{\text{quartz}}{8/7\ SiO_2} + 1/7\ H_2O\ , \tag{i}$$

$$\underset{\text{tremolite}}{1/5\ Ca_2Mg_5Si_8O_{22}(OH)_2} + \underset{\text{magnetite}}{Fe_3O_4} + \underset{\text{quartz}}{4/3\ SiO_2} + 1/3\ H_2O \rightarrow \underset{\text{hematite}}{Fe_2O_3} + \underset{\text{ferrotremolite}}{1/5\ Ca_2Fe_5Si_8O_{22}(OH)_2} + \underset{\text{talc}}{1/3\ Mg_3Si_4O_{10}(OH)_2}\ , \tag{j}$$

$$\underset{\text{ferrotremolite}}{1/5\ Ca_2Fe_5Si_8O_{22}(OH)_2} + \underset{\text{kupfferite}}{1/7\ Mg_7Si_8O_{22}(OH)_2} \rightarrow \underset{\text{tremolite}}{1/5\ Ca_2Mg_5Si_8O_{22}(OH)_2} + \underset{\text{grunerite}}{1/7\ Fe_7Si_8O_{22}(OH)_2}\ . \tag{k}$$

At constant temperature the corresponding equations and equilibrium constants are:

$$\frac{K_h}{P_{H_2O}^{4/21}} = X_{cum} \quad , \tag{10}$$

$$P_{H_2O}^{1/7} \; Ki = 1 - X_{cum} \quad , \tag{11}$$

$$\frac{K_j}{P_{H_2O}^{1/3}} = \frac{X_{act}}{1 - X_{act}} \quad , \tag{12}$$

$$K_k = \frac{X_{cum}(1-X_{act})}{X_{act}(1-X_{cum})} \quad , \tag{13}$$

$$K_h = \exp \frac{\Delta G_h^\circ}{RT} \quad , \quad K_i = \exp \frac{\Delta G_i^\circ}{RT} \quad ,$$

$$K_j = \exp \frac{\Delta G_j^\circ}{RT} \quad , \quad K_k = \exp \frac{\Delta G_k^\circ}{RT} \quad .$$

In these equations cummingtonite as well as actinolite is treated as an ideal solution since figure 4 seems to indicate that the deviation from ideality is not great. Not all four of these reactions are independent since (h) − (i) − (j) = (k); therefore $K_k = K_h/K_iK_j$. From the phase rule and equations (10) through (12) it is apparent that the compositions of actinolite and cummingtonite and P_{H_2O} are fixed at any given temperature. This is the same result as for assemblage B_1 which contains seven solid phases. Assemblage B_2 contains only six minerals, but since no solid carbonate phase is present, CO_2 does not enter into the reactions and may be dropped as a component. If present in the system, CO_2 merely acts as an inert gas with respect to the solid phases. It is also apparent that the cube of equation (12) for reaction (j) is identical to the transposed form of equation (7) of assemblage B_1. Since P_{H_2O} is the same function of $Mg/(Mg + Fe^{2+})$ in actinolite in both assemblages, the composition of actinolite in both assemblages should also be the same if the temperature and P_{H_2O} were the same where the two assemblages occur. This appears to explain the observed equality of $Mg/(Mg + Fe)$ in the actinolites of the two assemblages. Assemblages B_1 and B_2 occur in close proximity (some tens of feet) as observed in the field. It is therefore reasonable that the temperature and pressure of crystallization should have been very similar. Reference to figure 9 as well as consideration of the complete assemblages indicate that the two assemblages owe their origins to different bulk composition ranges.

Equation (13) is the simple ion exchange equation for ideal solutions and is analogous to equation (3). However, equation (13) does not describe the behavior of the solid solutions as well as equation (3) because of the apparent non-ideal behavior of cummingtonite. This may be seen by comparing figure 4 with figure 10.

In assemblage B_2 the following reactions apply:

$$\underset{\text{tremolite}}{1/5\ Ca_2Mg_5Si_8O_{22}(OH)_2} + \underset{\text{quartz}}{2/5\ SiO_2} + \underset{\text{calcite}}{3/5\ CaCO_3} \rightarrow \underset{\text{diopside}}{CaMgSi_2O_6} + 3/5\ CO_2 + 1/5\ H_2O \quad , \tag{1}$$

$$\underset{\text{ferrotremolite}}{1/5\ Ca_2Fe_5Si_8O_{22}(OH)_2} + \underset{\text{quartz}}{2/5\ SiO_2} + \underset{\text{calcite}}{3/5\ CaCO_3} \rightarrow \underset{\text{hedenbergite}}{CaFeSi_2O_6} + 3/5\ CO_2 + 1/5\ H_2O \quad , \tag{m}$$

$$\underset{\text{hedenbergite}}{CaFeSi_2O_6} + \underset{\text{hematite}}{Fe_2O_3} + CO_2 \rightarrow \underset{\text{magnetite}}{Fe_3O_4} + \underset{\text{quartz}}{2\ SiO_2} + \underset{\text{calcite}}{CaCO_3} \quad , \tag{n}$$

$$\underset{\text{ferrotremolite}}{1/5\ Ca_2Fe_5Si_8O_{22}(OH)_2} + \underset{\text{hematite}}{Fe_2O_3} + 2/5\ CO_2 \rightarrow \underset{\text{magnetite}}{Fe_3O_4} + \underset{\text{quartz}}{8/5\ SiO_2} + \underset{\text{calcite}}{2/5\ CaCO_3} + 1/5\ H_2O \quad . \tag{c}$$

The corresponding equations and equilibrium constants for constant temperature conditions are as follows:

$$P_{CO_2}^{3/5}\ P_{H_2O}^{1/5}\ K_l = \frac{X_{act}}{X_{Ca\text{-}px}} \quad , \tag{14}$$

$$P_{CO_2}^{3/5}\ P_{H_2O}^{1/5}\ K_m = \frac{1 - X_{act}}{1 - X_{Ca\text{-}px}} \quad , \tag{15}$$

$$\frac{K_n}{P_{CO_2}} = 1 - X_{Ca\text{-}px} \quad , \tag{16}$$

$$\frac{K_c\ P_{H_2O}^{1/5}}{P_{CO_2}^{2/5}} = 1 - X_{act} \quad , \tag{6}$$

$$K_l = \exp\frac{\Delta G_l^\circ}{RT} \quad , \quad K_m = \exp\frac{\Delta G_m^\circ}{RT} \quad ,$$

$$K_n = \exp\frac{\Delta G_n^\circ}{RT} \quad , \quad K_c = \exp\frac{\Delta G_c^\circ}{RT} \quad .$$

Only three of these reactions are independent, since $K_m = K_c/K_n$. An additional equation which might be written is that for the ion exchange reaction between actinolite and Ca-pyroxene; but this reaction is equal to the difference of reactions (l) and (m). It should be noted that although figure 2 implies that the relation $X_{act} = X_{Ca\text{-}px}$ might hold, this relation would not diminish the number of degrees of freedom of the system. Also, equation (6) again appears in this assemblage. Consequently if the temperature and the gas pressures were the same as in assemblages B_1 and B_2, the composition of actinolite should be the same in all three assemblages, as has been observed.

It was previously noted that assemblage B_3 and some specimens of assemblage B_1 appear to contain only one carbonate. This is somewhat doubtful in view of the insensitivity to small quantities of phases of the identification methods used. However, the fact that dolomite has not been observed to coexist with Ca-pyroxene (table 4), makes it seem likely that dolomite is not present in assemblage B_3.[1] If only one carbonate is present in these assemblages, they are divariant. The fact that Mg/(Mg + Fe) is the same in both assemblages implies that H_2O and CO_2 were fairly mobile, enabling uniform pressures of these gases to be established throughout fairly large regions. However, this conclusion depends on the actual sensitivity of the minerals to gas pressure changes. This factor can be evaluated only when the thermal properties of the minerals are known.

If any mineral which has been assumed to be of fixed composition in the preceding discussion is actually variable, the derived functions do not hold true, depending on the degree of variability. For example, magnetite may contain some Mg. In this case the partial pressure of oxygen would be a function of the composition of magnetite as well as of the temperature. Also talc probably contains some Fe^{2+} and calcite may contain Fe^{2+} and Mg. Undoubtedly the minerals also vary in the amounts of major constituents which are usually assumed to be constant. If the minor elements reach concentrations above indefinite and variable threshold values they may be expected to have significant effects on the equilibria by acting as additional components. The latter effect is not apparent in the B group of assemblages. The additional variation in major components will affect the forms of the theoretical functions but will not influence conclusions as to the variance of the system which are based on the phase rule.

It should be emphasized that the theoretical functions as written imply no more than trends expected from the law of mass action. The magnitude of the trends depend on the values of the thermal data which enter into the functions. Furthermore, the functions apply only to the observed assemblages and do not predict the advent of other assemblages. For example, curves such as figure 11, if they have any real existence at all, may be cut out in certain P-T ranges by the fields of unpredictable assemblages. The only justification for presenting such curves is the existence of the assemblages to which they refer.

[1] Small quantities may be present due to subsequent exsolution.

The effect of volume differences between solid reactants and products on the equilibria of the B group assemblages.—In the previous discussion it was assumed that the difference in volume between solid reactants and products did not affect the equilibria. As will be shown, significant volume changes occur in the reactions of interest. Therefore, the question is one of how these volume changes might cause variation in the mineral compositions. In the case of the univariant (constant temperature) equilibria represented by figure 11 the following reactions are pertinent:

$$\underset{\text{ferrotremolite}}{3/5\ Ca_2Fe_5Si_8O_{22}(OH)_2} + \underset{\text{hematite}}{3\ Fe_2O_3} + \underset{\text{talc}}{Mg_3Si_4O_{10}(OH)_2} \rightarrow$$

$$\underset{\text{tremolite}}{3/5\ Ca_2Mg_5Si_8O_{22}(OH)_2} + \underset{\text{magnetite}}{3\ Fe_3O_4} + \underset{\text{quartz}}{4\ SiO_2} + H_2O\ , \qquad \text{(o)}$$

$$\underset{\text{talc}}{1/2\ Mg_3Si_4O_{10}(OH)_2} + \underset{\text{calcite}}{CaCO_3} + \underset{\text{quartz}}{2\ SiO_2} + \underset{\text{magnetite}}{Fe_3O_4} \rightarrow$$

$$\underset{\text{tremolite}}{3/10\ Ca_2Mg_5Si_8O_{22}(OH)_2} + \underset{\text{ferrotremolite}}{1/5\ Ca_2Fe_5Si_8O_{22}(OH)_2} + \underset{\text{hematite}}{Fe_2O_3} + CO_2\ . \qquad \text{(p)}$$

These two reactions are combinations of reactions (b) and (c) and are represented by equations (7) and (8), which were previously derived in a different manner. The volume difference between the solid reactants and products of reaction (o) is approximately –10cc per mole H_2O. For reaction (p) the volume difference per mole CO_2 is approximately –24cc. These values were calculated from mineral densities given by Winchell (1951). The most obvious effect of the volume differences is the shift in the equilibrium curves induced by the total gas pressure. This shift is toward higher gas pressures in this case and occurs even when the pressure on all phases is the same. However, this effect would cause no observable differences in the mineral compositions if the gas pressures were uniform since the shift would then be the same in different parts of the formation. A second effect which might be expected to shift the curves is that of varying load pressure on the solid phases. This problem has been extensively discussed by Ramberg (1944), Thompson (1955), and Fyfe, Turner and Verhoogen (1958). The magnitude of the shift for differences in overburden may be determined from the following relation:

$$P^* = P \exp \frac{\Delta V_s \Delta P_s}{RT}\ .$$

Here ΔV_s represents the difference in volume between solid reactants and products, ΔP_s represents the difference in pressure which acts on the solid phases in two different parts of the formation; P represents the equilibrium gas pressure in one part of the formation, and P* that in the other part. At high gas pressures P and P* should be regarded as fugacities.

In the case of the Quebec iron formation a probable maximum for the difference in overburden separating the analyzed specimens is 1000 feet, although the average distance is much less than this. At an arbitrary equilibrium

temperature of 500°C and a rock density of 4 the 1000-foot difference in overburden gives the following relations for reactions (o) and (p):

$$P^*_{H_2O} = 1.02\ P_{H_2O} \quad ;$$

$$P^*_{CO_2} = 1.045\ P_{CO_2} \quad .$$

Reference to figure 11 shows that the maximum shift in the composition of actinolite would occur where the pressure curves are flattest. Because of the necessarily arbitrary construction of figure 11, this factor cannot be accurately evaluated. However, for any configuration of curves and for any pressure ranges near those given by figure 11, detectable shifts in composition induced by a 1000-foot difference in overburden would be confined to the immediate vicinity of a pressure minimum.

Structural evidence seems to indicate that of the 11 actinolites of assemblage B_1 (table 4) only specimens DH4-185, DH7-480, and DH11-200 were separated from the others by more than a few hundred feet of overburden. However, even their vertical separation from the others was probably less than 1000 feet. Of the 11 actinolites only specimens DH4-185 and DH7-480 show values of Mg/(Mg + Fe) whose difference from the others exceeds that attributable to the analytical precision. However, the "normal" composition of DH11-200 indicates that these differences may not be significant. In view of the many approximations and uncertainties involved it is difficult to arrive at an unambiguous conclusion. Yet the relatively constant composition of the actinolites of assemblage B_1 leads one to believe that differences in overburden had little, if any, effect on the mineral assemblages.

Strictly the variation in pressure due to overburden requires the introduction of another pressure variable into the phase rule, giving now $v = (c+3)-p$. However, if the additional variation is not detectable as discussed above, the effect may be disregarded, and the ordinary form of the rule, containing one pressure variable, may be used. The uniformity of composition of the actinolites of assemblages B_1, B_2, and B_3 is thus consistent with either constant temperature, gas pressures, and load pressures or with slight undetectable variations in these quantities.

Comparison of the A and B groups of assemblages.—The A group of assemblages appears to present greater complications than the B group, and no detailed treatment is attempted. Most of the variation in Mg/(Mg + Fe) of the silicates of the A group may be explained in terms of the phase rule since the specimens of these assemblages usually contain fewer phases (including the gaseous phase) then major components. In these cases the compositions of the phases are dependent on local bulk compositions. Assemblage A_1, however, contains as many phases as some assemblages of the B group. Most of the latter contain actinolites of fairly uniform Mg and Fe content, but A_1 does not. The orderly element distributions shown by the A group and the obvious limitations on the numbers of phases indicate that a high degree of equilibrium was attained. Also two mineral pairs from the B group appear to fall on the same curves with the A group. This suggests similar temperatures of crystallization for the two groups, but does not prove it, since the temperature sensitivities of the distribution functions are not known.

The most striking difference between the A and B groups is in the degree of oxidation indicated by the iron oxides they contain. In B the partial pressure of oxygen was probably controlled by the association of magnetite and hematite. In the A group this was not possible since magnetite is the only iron oxide phase. It is possible that this factor caused the variability in A_1.

In drill hole number 7 an interesting sequence is revealed in passing through the contact of the A and B groups of assemblages (table 4). Here assemblage B_1 is represented by specimen DH7-480 which contains the "normal" magnesium-rich actinolite of this assemblage. From figure 4 it is seen that a hypothetical cummingtonite in equilibrium with this actinolite would have $Mg/(Mg + Fe) = 0.74$. Two feet away across the contact in assemblage A_2 specimen DH7-482 contains a cummingtonite with $Mg/(Mg + Fe) = 0.62$. Two feet farther the rocks of A_2 contain a cummingtonite (DH7-484) with $Mg/(Mg + Fe) = 0.51$. Finally, roughly ten feet from the contact is found the most iron-rich cummingtonite (DH7-490) of the sequence with $Mg/(Mg + Fe) = 0.48$. It seems highly probable that this sequence represents some kind of a diffusion gradient of oxygen in the vicinity of the contact. If this is true, the fact that the compositional gradient was not levelled seems to imply that oxygen was not very mobile during metamorphism. This is in marked contrast to the apparently high mobility of H_2O and CO_2 deduced from assemblage B rocks.

Insufficient mobility of certain elements to establish equilibrium is also indicated by variations in the composition of mineral species found over even shorter distances. For example, the compositions of the cummingtonites in specimens B-22 and B-22A are notably different although they were separated by only six inches. All the analyzed pairs of coexisting minerals were obtained from volumes of less than several cubic inches. Throughout such small volumes equilibrium appears to have been closely approached.

The variation in composition of a given mineral species as discussed above provides an index of the radius of free diffusion at the time of crystallization. However, these data give little indication of the amount of diffusion which preceded final crystallization or of the distance over which diffusion extended.

The correlation, shown by the iron formation, of mineral compositions with the type of coexisting iron oxide appears to illustrate the importance of oxidation in petrogenesis. It seems worthwhile therefore to compare the A and B groups of assemblages in a more exact manner in terms of the law of mass action. The assemblages of particular interest are A_3, B_1, and B_4 since all of these contain actinolite and talc. Assemblage B_1 has already been discussed in terms of non-oxidative reactions. However, the following important oxidation reaction must also be considered in this assemblage:

$$\underset{\text{magnetite}}{Fe_3O_4} + 1/4\,O_2 \rightarrow 3/2\ \underset{\text{hematite}}{Fe_2O_3} \quad . \tag{q}$$

The corresponding equation of equilibrium may be written as follows:

$$\exp \frac{\Delta G^\circ_q}{RT} = P_{O_2}^{1/4} \quad . \tag{18}$$

In assemblage B_4 the following oxidation reaction must be considered:

$$\underset{\text{ferrotremolite}}{1/5\ Ca_2Fe_5Si_8O_{22}(OH)_2} + \underset{\text{talc}}{1/3\ Mg_3Si_4O_{10}(OH)_2} + 1/4\ O_2 \rightarrow \underset{\text{tremolite}}{1/5\ Ca_2Mg_5Si_8O_{22}(OH)_2} + \underset{\text{hematite}}{1/2\ Fe_2O_3} + \underset{\text{quartz}}{4/3\ SiO_2} + 1/3\ H_2O\ . \tag{r}$$

The equation of equilibrium for this reaction is

$$\frac{(P'_{H_2O})^{1/3}}{(P'_{O_2})^{1/4}} \exp\left(\frac{\Delta G_r^\circ}{RT}\right)' = \frac{1-X'_{act}}{X'_{act}}\ . \tag{19}$$

The primed quantities indicate that the reaction occurs in assemblage B_4 as distinguished from reactions occurring in other assemblages.

In assemblage A_5 the oxidation reaction and equation of equilibrium are as follows:

$$\underset{\text{ferrotremolite}}{1/5\ Ca_2Fe_5Si_8O_{22}(OH)_2} + \underset{\text{talc}}{1/3\ Mg_3Si_4O_{10}(OH)_2} + 1/6\ O_2 \rightarrow \underset{\text{tremolite}}{1/5\ Ca_2Mg_5Si_8O_{22}(OH)_2} + \underset{\text{magnetite}}{1/3\ Fe_3O_4} + \underset{\text{quartz}}{1/3\ SiO_2} + 1/3\ H_2O\ , \tag{s}$$

$$\frac{(P''_{H_2O})^{1/3}}{(P''_{O_2})^{1/6}} \exp\left(\frac{\Delta G_s^\circ}{RT}\right)'' = \frac{1-X''_{act}}{X''_{act}}\ . \tag{20}$$

Here the doubly-primed quantities indicate assemblage A_5.

Other reactions are of course possible in these assemblages, but the written reactions serve the present purpose. All four of these reactions in fact occur in assemblage B_1, as was mentioned previously. An additional reaction of B_1 is the non-oxidative reaction (o). If this reaction is divided by 3, the corresponding equilibrium equation is

$$P_{H_2O}^{1/3} \exp\frac{\Delta G_o^\circ}{3RT} = \frac{1-X_{act}}{X_{act}}\ . \tag{21}$$

This equation is identical to the cube root of equation (7). It is apparent that the reactions 1/3 (o), (r), and (s) differ only by multiples of reaction (q).

If it is now assumed that T, P_{H_2O}, and P_{CO_2} are everywhere the same in the region in which the three assemblages are found, division of equation (19) by equation (21) gives

$$\frac{(P'_{O_2})^{1/4} \exp\ (\Delta G_r^\circ/RT)}{\exp\ (1/3\ \Delta G_o^\circ/RT)} = \frac{X_{act}\ (1-X'_{act})}{X'_{act}\ (1-X_{act})}\ ,$$

where $P_{H_2O} = P'_{H_2O}$ and $T = T'$.

But this division also implies that

$$(r) - 1/3\ (o) = (q)\ ;$$

or

$$\frac{\exp\ (\Delta G_r^\circ/RT)}{\exp\ (1/3\ \Delta G_o^\circ/RT)} = \exp\frac{\Delta G_q^\circ}{RT} = P_{O_2}^{1/4}\ .$$

This gives

$$\frac{P^{1/4}_{O_2}}{(P'_{O_2})^{1/4}} = \frac{X_{act}\ (1 - X'_{act})}{X'_{act}\ (1 - X_{act})} \quad . \tag{22}$$

From this it is apparent that P'_{O_2} in assemblage B_4 is a function of the observed parameters X_{act} and X'_{act} and the known function of the temperature, ΔG_q°. Thus if the temperature were known P_{O_2} might be calculated from observed values of X_{act} and X'_{act}. Similar reasoning with respect to assemblage A_5 leads to the relation

$$\frac{P^{1/6}_{O_2}}{(P''_{O_2})^{1/6}} = \frac{X_{act}\ (1 - X''_{act})}{X''_{act}\ (1 - X_{act})} \quad , \tag{23}$$

where

$$P^{1/6}_{O_2} = \exp \frac{2\Delta G_q^\circ}{3RT} \quad .$$

The denominator of the left side of equation (22) must always exceed the numerator since P'_{O_2} lies on the hematite side of the boundary curve for reaction (q). The converse is true for equation (23). As was stated previously, P_{O_2} and X_{act} of assemblage B_1 are usually fixed at any given temperature by phase rule consideration. If the form of the phase rule $v = (c + 2) - p$ is applied to B_4 the variance is seen to be 3. This means that in addition to the temperature and total gas pressure an additional variable must be specified to fix the state of the system. Thus if X'_{act} is the additional variable specified, P'_{O_2} and all other variables are determined. In assemblage A_5 the variance is also 3 since CO_2 does not occur in a solid phase and so may be dropped as a component.

Reference to table 4 shows that $X''_{act} < X_{act} < X'_{act}$. This result is to be expected from equations (22) and (23) if the assumptions used in deriving these equations, namely that T, P_{H_2O}, and P_{CO_2} are the same in the three assemblages, are valid. The increase in P_{O_2} in the sequence of assemblages A_5, B_1, and B_4 as indicated by their coexisting oxides is thus also reflected in the ferromagnesian minerals. These same general relations might be expected to hold for all the assemblages since the oxidation reactions for all the ferromagnesian minerals are similar. The correlation, shown by figures 2, 3, 4, and 8, between the coexisting iron oxides and the compositions of the ferromagnesian minerals is thus readily explained since hematite should coexist with the most magnesium-rich silicates, other conditions being the same.

From the foregoing it is clear that there is a strong tendency to decrease the quantity of ferrous iron in ferromagnesian minerals as the partial pressure of oxygen is increased. In metamorphic rocks this appears to be accomplished by selective breakdown of the ferrous component to form higher oxides. This tendency may be opposed by other factors, notably the entropy of mixing of the solid solutions. Temperature or the pressures of other gases may or may not oppose it. In processes such as weathering the effect may be obscured by the decomposition of the entire mineral. The effect would also be obscured in

rocks which contain alkali metals and aluminum since these elements react to give ferric silicates.

SUMMARY OF THE METAMORPHISM OF THE IRON FORMATION

On the basis of the observed features and theoretical considerations it is possible to construct a model of the metamorphism. It is clear that the metamorphism was no isolated event, but rather a complex interaction of many processes. These processes acted upon the products of foregoing events which to a large extent controlled their direction. The initial event was the deposition of the sediments. From compositional evidence it is inferred that the mechanism of sedimentation was largely chemical rather than physical. Of the period which separated the original sediment from the culminating metamorphism even less can be inferred. However, it is possible that the iron formation underwent some oxidation before burial or before the culminating metamorphism. Similarly there may have been some rearrangement of material or compositional changes during diagenesis or previous metamorphism.

The critical factors which influenced the rock were not only pressure and temperature but also its own kinetic and structural properties. The preservation of the original sedimentary features are probably almost entirely due to kinetic restrictions on metamorphic processes such as chemical reactions and diffusion. The structural history accounts, in all probability, for many of the non-sedimentary features.

The culminating metamorphism fed upon products locally accumulated by other processes. Although physical variables such as temperature, load and structural pressures, and permeability probably largely determined the grade of metamorphism and general mineralogy, the minerals themselves probably also exercised control. The metamorphism as a whole must have been a degassing process and was therefore dependent upon the permeability of surrounding rocks. Loss of this permeability at any stage would have essentially closed the system, and metamorphism might have become self-regulatory. In this scheme the essentially univariant and divariant B group assemblages find a place. In most of these assemblages coexisting hematite and magnetite probably acted as buffers controlling oxygen pressure. The carbonate and silicates could have served the same purpose for H_2O and CO_2. However, this situation could obtain only in regions which contained the critical minerals. In regions which did not contain the right assemblages or in which certain minerals were used up in the reactions, the variance would have been increased to the extent that the mineral compositions no longer reflected the P-T conditions but were dependent on the local bulk compositions.

The orderly distribution of elements among coexisting minerals, the correlation of mineral compositions with the presence of hematite, and the general limitations on the numbers and types of minerals in association all indicate a close approach to chemical equilibrium during metamorphism. The fact that this equilibrium was confined to small volumes is readily explained by kinetics.

GENERAL CONCLUSIONS

Many of the features shown by the Quebec iron formation illustrate principles which appear to be applicable to other petrologic problems. The orderly element distribution and phase relationships are excellent criteria for equilibrium. Furthermore, the distribution relations themselves reflect the fundamental energetic properties of solid solutions and provide a means of studying these properties in systems which may be inaccessible to experimentation. One of the most important corollaries to the detection of an equilibrium relationship concerns the introduction of material. A mineral phase in equilibrium with the rest of the rock cannot have originated solely by replacement or void filling but must also have reacted with the entire rock. The application of this criterion to ore deposits of many kinds would form an interesting line of investigation. A further application of these criteria of equilibrium is in the study of a wide variety of plutonic and hypabyssal rocks. In such rocks the detection of equilibrium or disequilibrium relations is fundamental to the determination of the mode of origin. Other possible applications involve the interrelation of thermodynamics and kinetics. In this sense a rock may be regarded as a continuum of interpenetrating leaky crucibles, the walls of these crucibles being the kinetic barriers to diffusion which prevent the spread of chemical equilibrium. The geometry and dimensions of these crucibles would seem to be important measurable parameters of any rock.

ACKNOWLEDGMENTS

The writer is pleased to acknowledge the advice and encouragement given by Hans Ramberg throughout the course of this study. Thanks are also due to George DeVore, Julian Goldsmith, E. Hellner, and John Jamieson for reading the manuscript, to Oiva Joensuu for much advice on the analytical methods, and to Edward Olsen and Sigurd Rutlin for help with some of the analytical work. The writer is grateful for the opportunity to have participated in many stimulating discussions with Ralph Kretz and Sisir Sen. The specimens for this study were made available through the generous cooperation of the Jones & Laughlin Steel Corporation and its geological staff. Financial assistance was provided by three Standard Oil Company of California fellowships.

REFERENCES

Foslie, S., 1945, Hastingsites and amphiboles from the edipote amphibolite facies: Norsk Geol. Tidssk., v. 25, p. 74-96.

Fyfe, W. S., Turner, F. J., and Verhoogen, J., 1958, Metamorphic reactions and metamorphic facies: Geol. Soc. America Mem. 73.

Goldschmidt, V. M., 1911, Die Kontaktmetamorphose in Kristianiagebiete: Videnskskrifter I. Mat.-naturv. Kl., no. 11.

Goldsmith, J. R., Graf, D. L., and Joensuu, O. I., 1955, The occurrence of magnesian calcites in nature: Geochim. et Cosmochim. Acta, v. 7, p. 212-230.

Gross, G. A., 1955, The metamorphic rocks of the Mount Wright and Matonipi Lake areas of Quebec: Unpublished Ph.D. thesis, University of Wisconsin.

Harker, A., 1932, Metamorphism: London, Methuen.

Hill, A. E., Durham, G. S., and Ricci, J. E., 1940, Distribution of isomorphous salts in solubility equilibrium between liquid and solid phases: Am. Chem. Soc. Jour., v. 62, p. 2723-2732.

Howie, R. A., 1955, The geochemistry of the Charnockite Series of Madras, India: Royal Soc. Edinburgh Trans., v. 62, p. 725-768.

Irving, R. D. and Van Hise, C. R., 1892, The Penokee iron-bearing series of Michigan and Wisconsin: U. S. Geol. Survey Mon., v. 19.

Kretz, R., 1959, A chemical study of garnet, biotite, and hornblende from gneisses of southwestern Quebec, with emphasis on the distribution of elements in coexisting minerals: Jour. Geology, v. 67, p. 371-402.

Ramberg, H., 1944, Relation between external pressure and vapor tension of compounds, and some geological implications: Norsk Videnskaps. Akad. Oslo. Avh. I Mat.-naturv. Kl., no. 3.

———, 1952, The origin of metamorphic and metasomatic rocks: Chicago, Univ. Chicago Press.

Ramberg, H. and DeVore, G. W., 1951, The distribution of Fe^{++} and Mg^{++} in coexisting olivines and pyroxenes: Jour. Geology, v. 59, p. 193-210.

Rankama, K. and Sahama, Th. G., 1949, Geochemistry: Chicago, Univ. Chicago Press.

Sahama, Th. G. and Torgeson, D. R., 1949, Some samples of the applications of thermochemistry to petrology: Jour. Geology, v. 57, p. 255-262.

Thompson, J. B., 1955, The thermodynamic basis for the mineral facies concept: Am. Jour. Sci., v. 253, p. 65-103.

Winchell, A. N. and Winchell, H., 1951, Elements of optical mineralogy, Part II: New York, John Wiley and Sons, Inc.

[American Journal of Science, Vol. 258, Summer 1960, P. 498-517]

EXPERIMENTAL INVESTIGATION OF SILICATE SYSTEMS CONTAINING TWO VOLATILE COMPONENTS PART I. GEOMETRICAL CONSIDERATIONS*

P. J. WYLLIE[1] and O. F. TUTTLE

Division of Earth Sciences, College of Mineral Industries
The Pennsylvania State University

ABSTRACT. This is the first in a series of papers describing the effects of volatile materials, in addition to water, on the melting temperatures of albite and granite. In order to understand the results obtained, familiarity with the geometry of ternary isobaric (TX) prisms is required. A detailed description of the PTX model for the system albite-water is followed by description of the phase spaces, surfaces and lines in the TX prisms produced by adding a second volatile, C, to the components albite-water. The shape of the liquidus field boundary depends upon the solubilities of water, C, and mixtures of water and C in the silicate liquid. At constant pressure, the second volatile C may raise or lower the melting temperature in a binary silicate-water system. Possible arrangements of the liquidus and vaporus field boundaries between the bounding binary systems albite-water and albite-C are: (1) they pass continuously in temperature and composition from one binary system to the other, (2) they have a temperature maximum, and (3) they have a temperature minimum. These types will serve as models for the experimental data in later papers in the series. Published data in the systems albite-H_2O-CO_2, "granite"-H_2O-CO_2 and CaO-CO_2-H_2O are compared with the models described.

INTRODUCTION

Although considerable data are now available on the melting relations in silicate systems with water as a volatile component, little is known of the effect of other volatile materials. Petrologists have long been aware that mineralizers, in addition to water, play an important role in the processes of formation and alteration of igneous and metamorphic rocks and related ore deposits, and this study was undertaken to investigate the melting relations in silicate systems containing water and a second volatile.

This is the first in a series of papers describing the effects of water together with volatile materials such as CO_2, HF, NH_3, HCl, SO_3 and P_2O_5. The results will be presented as projections from within ternary isobaric (TX) prisms and, in order to understand them, familiarity with the geometry of the prisms is required. Indeed, before successful experimentation can be planned in such systems, it is necessary to know the general arrangement of lines, surfaces and spaces within the prisms used to depict the phase relations. We are not concerned here with theoretical aspects of phase equilibria, but only with the geometry of phase fields in three-dimensional models. We hope that geologists, accustomed to working with three-dimensional problems, will have no difficulty in visualizing the general relations described below.

Before taking up the phase relations in systems with two volatile components, we will discuss the equilibrium relations in the binary system albite-water. This will serve as a general example of systems containing water and a rock-forming silicate, and it will represent one side of the ternary systems to be described later. Considerable space will be devoted to this elementary

* Mineral Industries Experiment Station Contribution No. 58-137.

[1] Now at the School of Chemistry, University of Leeds.

example, as an understanding of the binary system is a prerequisite for the ternary systems which follow.

This work has been supported by the National Science Foundation. Our thanks are due to J. W. Greig and R. Roy for discussion of various aspects of the theoretical and practical problems involved in the study.

SYSTEM ALBITE-WATER

Phase equilibrium relations in a one-component system can be defined by fixing the two variables pressure and temperature, and the familiar PT diagram is a phase diagram for such a system. For a binary system, with the added variable composition, a three-dimensional model is required to depict the phase relations. This PTX model or phase diagram can be thought of as two parallel PT planes, one for each one-component system, separated by a coordinate giving composition. The model for the system albite-water is shown in figure 2A.

It is customary for the compositions of mixtures in silicate systems with or without volatile components to be expressed in terms of weight percentages, and in many "dry" systems the representations by weight or molecular percentages differ only slightly. However, the molecular weights of volatile components such as water are very much smaller than those of the silicate

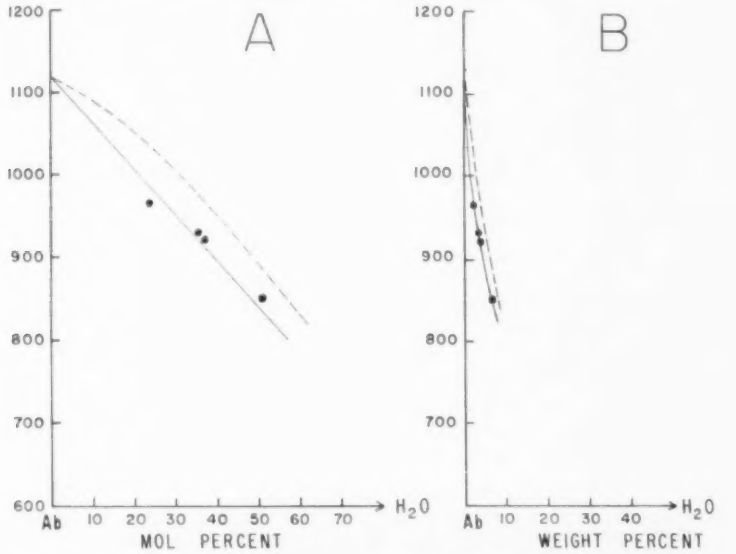

Fig. 1. The system albite-water. TX projections for *univariant* liquids in the three-phase equilibrium vapor + liquid + albite, with compositions expressed in molecular percentages (1A) and in weight percentages (1B). The solid circles are points determined by Tuttle and Bowen (1958), and the dotted lines represent the results of Goranson (1938). In fig. 1A, the line showing the compositions of the *univariant* liquids at different temperatures, if extended, would intersect the H_2O axis above the critical point of water.

components, and the phase diagrams for systems containing volatiles differ considerably from each other when expressed in molecular percentages or in weight percentages. For example, in the molecular percentage TX diagram (fig. 1A) the curve giving the compositions of albite-rich liquids in equilibrium with vapor and albite, if extended to the water ordinate, would clearly intersect it well above the critical temperature of water (374°C). Extension of the same curve on the weight per cent diagram (fig. 1B) would give no indication of this relationship. Molecular percentages will be used throughout this discussion.

Hypothetical PTX diagrams for systems of this type, with pure compounds as the only crystalline phases, have been presented and described by Boeke and Eitel (1923), Niggli (1937), Tunell (1950), and Ricci (1951). All of these presentations are well illustrated . .d described but, as they are hypothetical, they differ significantly from the silicate-water systems in which we are interested. Although we are not concerned here with phase relations below the critical point of water, for completeness we will describe this part of the system.

Construction of the PTX model (fig. 2) was based, as far as possible, on experimentally determined points (Goranson, 1938; Bowen and Tuttle, 1950;

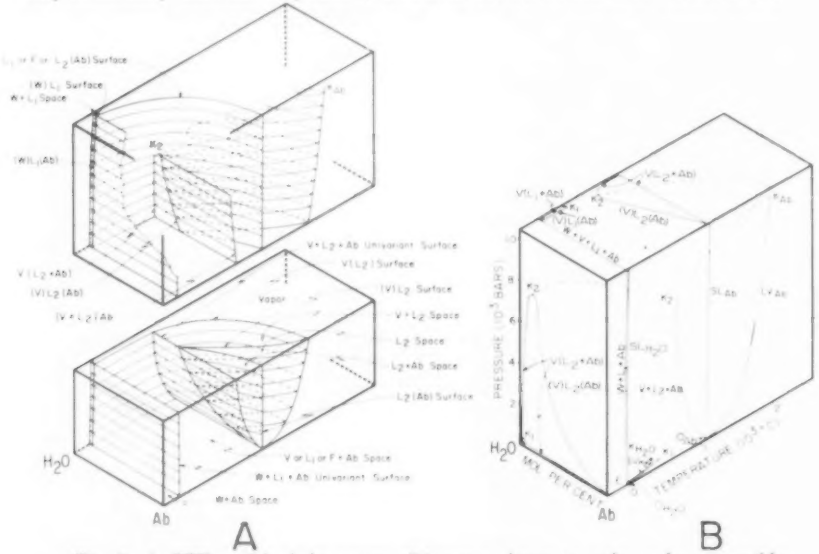

Fig. 2. A. PTX model of the system albite-water drawn to scale, as far as possible. Much of the diagram is based on experimentally determined points, but parts are inferred, and parts are schematic; the diagram is distorted near the H_2O side in order to show the phase relations. The model has been drawn in two parts, thus exposing one of the isobaric sections used to contour the phase surfaces.

B. Projections of *univariant* lines from within the PTX model onto the PT, PX, and TX faces. The dotted lines represent the critical curve. The critical point of albite, K_{Ab}, is not known, and the critical pressure could be less than the pressure of the second critical end-point, K_2.

Morey, 1957; Tuttle and Bowen, 1958), and on reasonable extrapolations from these points. It should be kept in mind that some of the relations are inferred, and in the region near the critical point of albite the relations are purely schematic. The critical curve joining the critical points of albite and water is schematic, but it will have the general form shown in the projections. The univariant PT relations for solid + liquid and liquid + vapor for water are well established experimentally, and the solid + liquid curve for albite can be calculated; the albite liquid + vapor curve is schematic.[2] All of the diagrams have been distorted to show the phase relations near the water side, because the solubility of albite in water, even at high temperatures, is so small that it cannot be represented on this scale.

At low pressures, Morey (1957) found that albite was decomposed by hot water, with the alkali oxide and silica being extracted at a greater rate than alumina. The amount of decomposition decreased at higher pressure, until at 2000 bars none could be detected. Parts of the system are therefore not truly binary. At higher temperatures, the silicate liquid may be decomposed by the aqueous vapor, but no data are yet available on the compositions of vapors co-existing with silicate liquids. In the present discussion it is assumed that the system remains binary.

A description of the phase relations can be considerably simplified by using abbreviations. Accordingly, the following will be used:

Ab = crystalline albite
W = ice
S = solid
L = liquid
L_1 = low temperature liquid
L_2 = high temperature liquid
V = vapor
F = fluid
O = triple-point in one-component system
E = eutectic
K = critical point or critical end-point
$V + L_1$ = vapor and liquid in equilibrium
$V(L_1)$ = vapor which can co-exist with liquid
$(V)L_1$ = liquid which can co-exist with vapor
$(V)L_1 + Ab$ = liquid and albite crystals which can co-exist with vapor
$(V)L_1(Ab)$ = liquid which can co-exist with albite crystals and vapor
$W(V + L_1)$ = ice crystals which can co-exist with vapor and liquid, etc.

The order in which the letters appear from left to right indicates decreasing water content.

PT, PX, and TX projections.—The PTX model is made up of spaces, separated by surfaces and lines (figs. 2A and 3A). In figures 2B and 3B, the *univariant* lines have been projected from within the PTX model onto the PT, PX, and TX faces. Figure 2 has been drawn as nearly as possible to scale, although as mentioned earlier the diagram is distorted to show the relations

[2] In practice, albite liquid would probably dissociate on boiling, so the liquid + vapor curve would have no real existence in the one-component system albite.

between H_2O-rich liquids and vapors. Despite this distortion it is impossible to show the relations in detail near the triple point of H_2O and the eutectic (E), and these are illustrated schematically in figure 3.

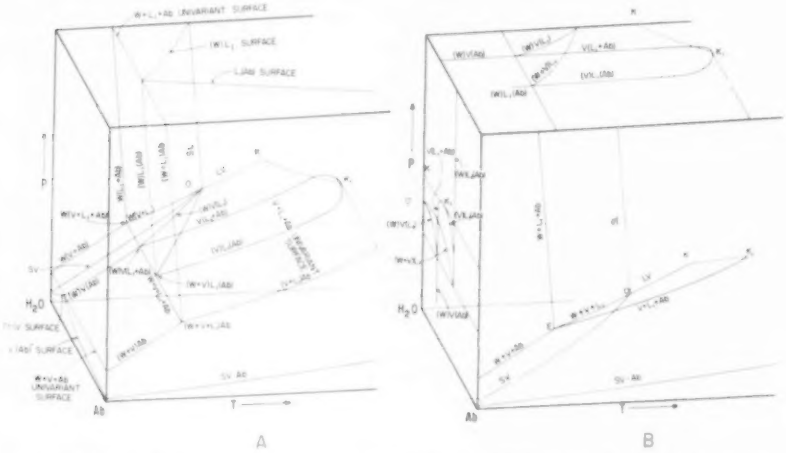

Fig. 3. A. Greatly distorted PTX model of the low-temperature region in the system albite-water, illustrating the manner in which four *univariant* three-phase surfaces (each containing three *univariant* lines) meet along the *invariant* eutectic line where four phases co-exist at equilibrium. SV.Ab is the sublimation curve for albite. Three of the *univariant* surfaces are labeled: the fourth is the small triangular surface extending from O to the eutectic line. The dotted line is the critical curve.

B. Projections of *univariant* lines from within the PTX model onto the PT, PX, and TX faces.

In the PT projection (figs. 2B and 3B), four *univariant* curves meet at the triple-point of each component (O_{H_2O}, O_{Ab}). The curves are: (1) Sublimation, SV_{H_2O} and SV_{Ab}, (2) melting, SL_{H_2O} and SL_{Ab}, (3) vapor pressure, LV_{H_2O} and LV_{Ab}, and (4) the binary *univariant* three-phase solubility curves W + V + L_1 and V + L_2 + Ab. With the scale used in figure 2, the triple-points and sublimation curves lie effectively on the base of the PTX model.

At a temperature slightly below the triple-point of H_2O, there is a eutectic (the only *invariant* point in the binary system which will be considered in detail[2]) at which the four phases, W + V + L_1 + Ab can exist in equilibrium. The two *univariant* PT solubility curves, W + V + L_1 and V + L_1 + Ab, meet at the eutectic (fig. 3B). The former extends from the triple point of H_2O to the eutectic, and the latter from the eutectic to the first critical end-point (K_1). At the second critical end-point (K_2) the solubility curve V + L_2 + Ab appears (fig. 2B), and continues to the triple-point of Ab. L_1 and L_2 are, respectively, the low temperature aqueous liquid and the high temperature silicate liquid.

[2] For the purpose of discussion it is assumed that water is insoluble in albite and does not react with it to produce other phases. Polymorphism in ice and albite will give rise to other invariant points, but these will be ignored in this description.

Critical end-points, K_1 and K_2, occur in this system, and in other binary systems where the silicate is only slightly soluble in H_2O, because the vapor pressure of saturated solutions rises high enough for the solubility curve, V + L + Ab, to intersect the critical curve, $K_{Ab}K_{H_2O}$. At the points of intersection, two saturated solutions of different compositions reach their critical temperatures and pressures, producing the first and second critical end-points. In the PTX region between the end-points the phase present is indeterminate between a liquid and vapor, but it may pass continuously into liquid or vapor by changing the PT conditions. Such a phase is sometimes called a fluid. Near the critical end-points properties of the liquid, vapor, and fluid phases may vary greatly with slight changes in P and T. Considerable extrapolation was required to estimate the position of K_2, and future experimental work may prove that it lies at a higher pressure than indicated.

Each of the PT curves of binary *univariant* three-phase equilibria (the solubility curves) is represented in PX and TX projections by three *univariant* curves. For example, the PT curve V + L_2 + Ab (fig. 2B) is represented in PX and TX by the curves V(L_2 + Ab), (V)L_2(Ab) and (V + L_2)Ab, which give the composition, pressure, and temperature of the three co-existing phases. (V + L_2)Ab falls on the Ab axis because H_2O is assumed to be insoluble in crystalline Ab. Similarly, the PT curve W + V + L_1 (fig. 3B) is represented in PX and TX by the curves W(V + L_1), (W)V(L_1), and (W + V)L_1, and the PT curve V + L_1 + Ab is represented in PX and TX by the curves V(L_1 + Ab), (V)L_1(Ab) and (V + L_1)Ab. The curves W(V + L_1) and (V + L_1)Ab fall on the H_2O and Ab axes, respectively.

The eutectic E (fig. 3B), a point in PT projection, is represented in PX and TX by four points on a line, the points giving the compositions of the four phases which co-exist at the eutectic pressure and temperature. The points are W(V + L_1 + Ab), (W)V(L_1 + Ab), (W + V)L_1(Ab) and (W + V + L_1)Ab (fig. 3A). Each point lies at the intersection of three *univariant* curves. The three curves for each of the points W(V + L_1 + Ab) and (W + V + L_1)Ab degenerate to single straight lines in PX and TX because W or H_2O and Ab are assumed to be insoluble in each other.

The compositions of co-existing liquids and vapors in equilibrium with W or Ab along the *univariant* PT curves W + V + L_1, V + L_1 + Ab and V + L_2 + Ab can be found in the PX and TX projections by the intersections of straight lines parallel to the X-axis with the curves (W)V(L_1) and (W + V)L_1, or V(L + Ab) and (V)L(Ab). In the PX projection of figure 2B, the curve V(L_2 + Ab), extending from the second critical end-point (K_2) to the triple point of Ab(O_{Ab}), crosses the curves V(L_1 + Ab) and (V)L_1(Ab) in projection only. This can be seen in the TX projection where the curves do not intersect.

The *univariant* lines illustrated in the projections lie on surfaces within the PTX model, and we turn now to a description of the model.

PTX model.—The solid model is made up of spaces representing conditions of pressure, temperature, and composition which give the phase or phases illustrated in figures 2 through 4. The model contains two types of space: *trivariant* space in which only one phase is stable, and *divariant* space

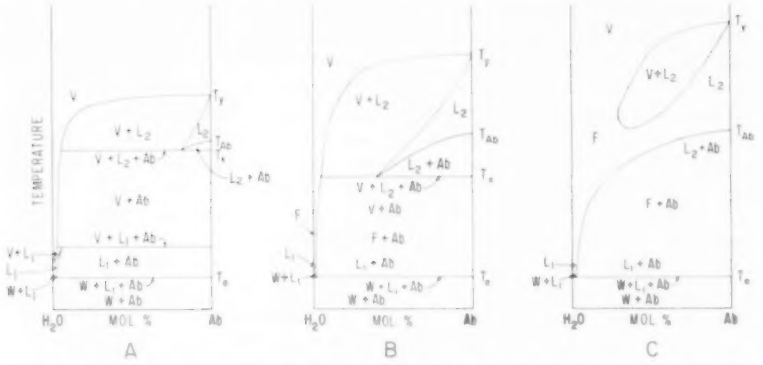

Fig. 4. Isobaric sections through the PTX model for the system albite-water. The diagrams are distorted near H_2O in order to show the phase relations.

A. Pressure between O_{H2O} and K_{H2O}. At the first critical end-point, K_1, V = L_2 in the three-phase equilibrium V + L_1 + Ab.

B. Pressure between K_1 and K_2. This corresponds to the section exposed in fig. 2A. At K_2, V = L_2 in the three-phase equilibrium V + L_2 + Ab.

C. Pressure greater than K_2 (schematic).

in which two phases are stable at equilibrium. These two types of spaces are separated from each other by *divariant* curved surfaces which give the compositions, temperatures, and pressures at which one phase whose composition falls on a surface can co-exist with a second phase at equilibrium; the co-existing phase lies on a second *divariant* surface. These *divariant* surfaces intersect along *univariant* lines giving the PTX conditions under which the phase common to both surfaces can co-exist in equilibrium with two other phases. For example, the curved surfaces (V)L_2 and L_2(Ab) intersect along the curved line (V)L_2(Ab) (fig. 2A); the curved surfaces V(L_2) and V(Ab) intersect along the curved line V(L_2 + Ab); and the surfaces (V)Ab and (L_2)Ab intersect along the line (V + L_2)Ab.[4] These three curved lines, V(L_2 + Ab), (V)L_2(Ab), and (V + L_2)Ab are the lines which appear in PT projection as the single solubility curve, V + L_2 + Ab (fig. 2B).

At a fixed pressure in a binary system, any three phases can co-exist at only one temperature. The co-existing phases V, L_2, and Ab therefore lie on a series of straight lines parallel to the X-axis and perpendicular to the P– and T–axes of the solid model. These lines generate a *univariant* ruled surface, V + L_2 + Ab which, of course, contains the three *univariant* curved lines V(L_2 + Ab), (V)L_2(Ab) and (V + L_2)Ab (fig. 2A). The solubility curve, V + L_2 + Ab, in PT projection (fig. 2B) is thus a projection of the *univariant* ruled surface, containing three *univariant* curved lines. This *univariant* ruled surface separates *divariant* two-phase spaces, whereas the *divariant* curved surfaces separate *trivariant* one-phase spaces from *divariant* two-phase spaces.

[4] As water is insoluble in crystalline albite, the surfaces (L_2)Ab and (V)Ab lie in the albite PT plane, and they do not separate two spaces, like the other *divariant* surfaces, because the Ab space has degenerated to a plane.

Similarly, the other three-phase lines in the PT projection (fig. 3B) represent *univariant* ruled surfaces, each containing three *univariant* curved lines. Four ruled surfaces intersect at the eutectic, E, giving rise to an *invariant* line (the eutectic line in fig. 3A), along which four phases may co-exist at equilibrium. The relationships of the *univariant* lines and surfaces to the *invariant* eutectic line are illustrated in the greatly distorted figure 3A, and figure 4A shows the phase fields intersected by an isobaric section between the triple point (O_{H2O}) and the critical point (K_{H2O}) of H_2O.

We have referred to the low temperature and high temperature liquids L_1 and L_2 as if each occupied a different *trivariant* space. In a similar system without critical end-points, there would be only one *trivariant* liquid space, and although in the present example the L_1 and L_2 spaces are separated within the PTX model, they are not separated from each other by phase boundaries. It is possible to pass continuously from L_1, through fluid, to L_2 by varying simultaneously the pressure, temperature, and composition. Similar considerations apply to the *divariant* spaces L_1 + Ab and L_2 + Ab, and figure 2A shows the continuity of the *divariant surfaces* L_1(Ab) and L_2(Ab). On the other hand, the *divariant* spaces V + L_1 and V + L_2 are not continuous through the fluid region but form distinct closed spaces. In the region of critical points, the surfaces V(L) and (V)L become continuous with each other as shown for L_1 in figure 3B, and for L_2 in figure 2B. The *univariant* ruled surfaces V + L_1 + Ab and V + L_2 + Ab are really parts of the same surface, separated by the intervention of critical phenomena, and this applies to the *univariant* curved lines on the ruled surfaces. Above the first critical end-point a fluid solution co-exists with Ab as shown in figure 2A and in the isobaric sections, figures 4B and 4C.

Keeping in mind the fact that some of the surfaces and spaces involving the liquids L_1 and L_2 are, in reality, continuous through the PTX model, we may summarize the elements of the three-dimentional model:

Three *trivariant* spaces, V, L_1, L_2.

Eight *divariant* two-phase spaces: W + V, W + L_1, W + Ab, V + L_1, V + L_2, V + Ab, L_1 + Ab, L_2 + Ab.

Nine *divariant* curved surfaces: (W)V, (W)L_1, V(Ab), L_1(Ab), L_2(Ab), V(L_1), (V)L_1, V(L_2), (V)L_2.

Five *univariant* ruled surfaces: W + V + Ab, W + L_1 + Ab, W + V + L_1, V + L_1 + Ab, V + L_2 + Ab.

Fifteen *univariant* curved lines: W(V + Ab), (W)V(Ab), (W + V)Ab, W(L_1 + Ab), (W)L_1(Ab), (W + L_1)Ab, W(V + L_1), (W)V(L_1), (W + V)L_1, V(L_1 + Ab), (V)L_1(Ab), (V + L_1)Ab, V(L_2 + Ab), (V)L_2(Ab), (V + L_2)Ab.

One *invariant* line: W + V + L_1 + Ab.

Four *invariant* points: W(V + L_1 + Ab), (W)V(L_1 + Ab), (W + V)L_1(Ab), (W + V + L_1)Ab.

Two *critical end-points*, K_1 and K_2, each representing a composition, pressure, and temperature at which a critical solution may co-exist with Ab at equilibrium.

Isobaric sections.—The arrangement of spaces, surfaces, and lines within the PTX model can most easily be visualized with the aid of isobaric or isothermal sections through the model. Since it is convenient experimentally to work at constant pressure, we will limit discussion to isobaric sections. The PTX model (fig. 2A) was prepared by stacking a series of isobaric sections one above the other, and the model has been drawn in two parts to expose one of the sections between the first and second critical end-points. A similar section is illustrated in figure 4B. Figures 4A and 4C show sections between Ou_{2^0} and Ku_{2^0}, and above K_2.

Isobaric sections intersect the spaces in areas, the *divariant* curved surfaces in curved lines, the *univariant* ruled surfaces in straight lines, and the *univariant* curved lines in points where the intersections of *divariant* surfaces (curved lines) meet. In figure 4A, three one-phase spaces, seven two-phase spaces, three ruled surfaces, eight curved surfaces and nine curved lines are intersected. At pressures represented by the isobars, T_{Ab} is the melting point of Ab, T_y the boiling point of Ab, T_x the temperature at which V, L_2, and Ab co-exist and T_e the temperature at which W, L_1, and Ab co-exist. The diagrams are based on the available experimentally determined points, although they have been distorted to show the relations near the H_2O side-line. For instance, the area representing the space L_1 in figure 4A is really indistinguishable from the H_2O composition axis (Morey, 1957). At the pressure of the first critical end-point, K_1, $V = L_1$ in the three-phase equilibrium $V + L_1 + Ab$ (figs. 4A and 3A), and at the pressure of the second critical end-point K_2, $V = L_2$ in the three-phase equilibrium $V + L_2 + Ab$ (figs. 4B and 2A).

Experimentally, we are concerned with liquids at magmatic temperatures, and we are thus interested in only a few of the spaces, surfaces, and lines described above, namely, those on and adjacent to the *univariant* ruled surface $V + L_2 + Ab$. The low temperature T_e is of no interest in the present study, although the aqueous solution L_1 is, of course, geologically important; the high temperature T_y is beyond the reach of the experimental methods employed.

The purpose of the next section is to describe the phase relations when a second volatile component is added to the binary equilibria described above.

TERNARY SYSTEMS CONTAINING TWO VOLATILE COMPONENTS

Three-dimensional diagrams are required to illustrate the phase relations in a binary system, and the addition of a third component adds another dimension. In order to represent the ternary phase relations in three dimensions, one of the variables P, T, and X, must be fixed. Isobaric diagrams will be used, because it is convenient experimentally to keep pressure constant.

In the following pages, the low temperature liquid L_1 will not be considered, and the liquid L_2 will be designated L. The distinction between vapor, fluid, and liquid has been discussed above and for convenience both fluid and vapor will hereafter be indicated by V.

Most of the experimental data were obtained at a pressure of 2750 bars, and this falls between the first and second critical end-points in the system Ab–H_2O. In a discussion of the ternary system it is assumed that addition of the second volatile C does not change this condition.

Ternary phase relations.—Equilibrium conditions in the ternary system Ab–H_2O–C, at constant pressure, may be represented in a ternary isobaric (TX) prism (fig. 5A), whose base is an equilateral triangle with corners representing the three components. Temperature axes form the edges of the prism, and the three sides are isobaric TX sections through the binary PTX models for the systems Ab–H_2O, Ab–C, and H_2O–C.

At the pressure of the isobar, both H_2O and C are well above their critical points, and it is assumed that they are miscible in all proportions in the fluid phase, V. The H_2O–C face of the TX prism thus contains no phase boundaries. The Ab–H_2O face is illustrated in figures 4B, 5A, and 5B, and the Ab–C face will have the same general form as Ab–H_2O (figs. 5A, and 5D). Temperatures T_y and T_{Ab} are the same in both isobaric sections, but in the system Ab–C the temperature T_x, the solubility of C in the liquid (V)L(Ab), and the solubility of Ab in V(L + Ab) will differ from the corresponding values in the system Ab–H_2O.

The phase fields, phase boundaries, and isobaric *invariant* points of the two binary isobaric sections Ab–H_2O and Ab–C are connected through the ternary prism by phase spaces, phase surfaces and field boundaries. In each binary system, the three-phase equilibrium V + L + Ab is represented by an isobaric *invariant* straight line. As this three-phase equilibrium moves into the TX prism upon addition of the third component, the line becomes a three-phase triangle, the corners of which generate the three field boundaries, and the sides of which generate three two-phase ruled surfaces enclosing the three-phase space V + L + Ab (fig. 5A).

In figure 5A, the spaces, surfaces, and lines passing through the prism may be traced from the binary system Ab–C to Ab–H_2O. Figure 5C is a section through the prism from Ab to the composition $(H_2O)_{50}C_{50}$, which intersects the elements passing through the prism. These are:

One-phase spaces: V, L, and Ab [Ab reduces to a straight vertical line, assuming no solid solution of volatiles in Ab].

Two-phase spaces: L + Ab, V + L, V + Ab.

Three-phase space: V + L + Ab.

One-phase surfaces: (L)Ab, L(Ab), (V)L, V(L), (V)Ab, V(Ab). [(L)Ab and (V)Ab reduce to straight lines].

Two-phase surfaces: V(L)Ab, (V)L + Ab, V + L(Ab).

Field boundaries: (V + L)Ab, (V)L(Ab), V(L + Ab). [(V + L)Ab reduces to a straight line].

Figure 5C is not a binary system, of course, because the compositions of co-existing liquids and vapors do not lie in the plane of the section; it simply shows the phase fields intersected by the plane. The field boundaries intersect it in piercing points; *l* is the piercing point of the liquidus field boundary, (V)L(Ab), and the other point in figure 5C where four lines (intersected surfaces) meet is the piercing point of the vaporus field boundary, V(L + Ab).

The two-phase spaces are filled with tie-lines, joining the two phases which can co-exist at equilibrium (each phase lies on a one-phase surface). The sides of the three-phase triangles are limiting cases of these tie-lines, connecting L

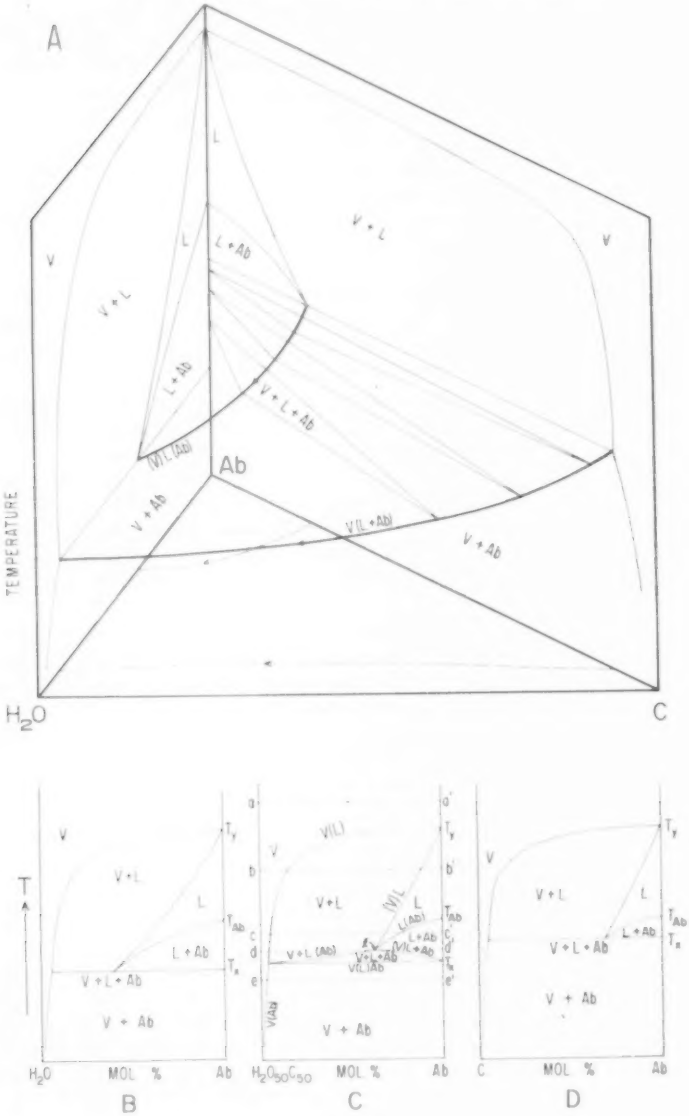
A
V
L
L + Ab
V + L
V + L + Ab
V (L) Ab
Ab
V + Ab
V (L + Ab)
TEMPERATURE
H2O
C
T
V + L
L + Ab
V + L + Ab
V + Ab
MOL %
B
V (L)
V (L) (Ab)
V (L) Ab
C
D

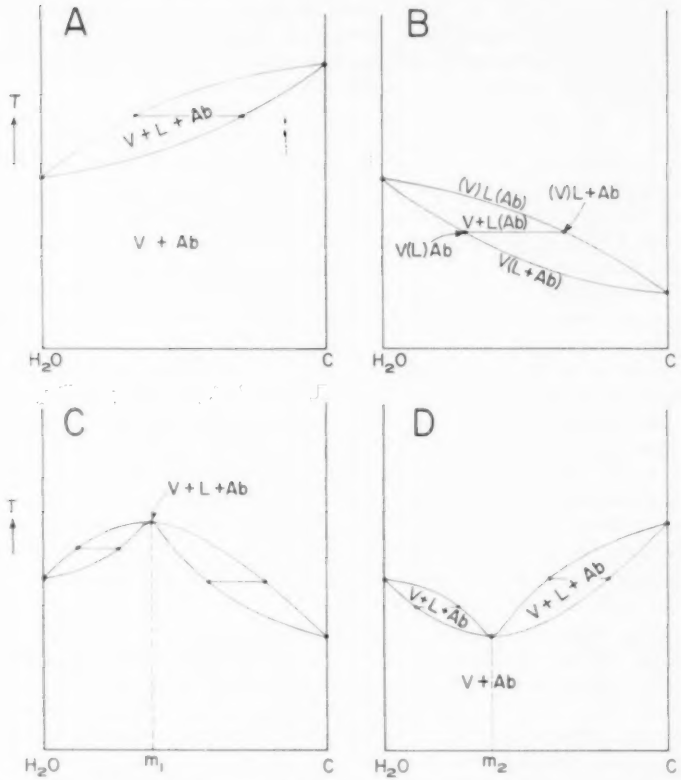

Fig. 6. Schematic perspective TX projections of liquidus and vaporus field boundaries, and three-phase triangles from within ternary isobaric prisms. The diagrams show the proportions of H_2O and C in liquids and vapors, without representing the proportion of Ab. The ordinates are thus projections of the binary systems Ab-H_2O and Ab-C. A, B, C, and D show four possible arrangements of the field boundaries. Three-phase triangles project as horizontal lines connecting pairs of points on liquidus and vaporus boundaries.

Fig. 5. Schematic ternary isobaric (TX) prism for the system Ab-H_2O-C, where C is a volatile component. The diagram shows the liquidus and vaporus field boundaries passing through the prism, as well as three three-phase triangles. The dotted lines are projections of the field boundaries onto the base of the prism (see fig. 7A).

B. Isobaric section through the PTX model of the system Ab-H_2O; this forms one side of the prism.

C. Vertical section through the prism above the line Ab-$(H_2O)_{50}C_{50}$, showing the spaces, surfaces, and lines passing through the prism. Spaces are intersected by the vertical plane in areas, surfaces in lines, and lines in points. For instance, the point l is the piercing point of the liquidus field boundary. When vapor and liquid co-exist, their compositions do not lie in this vertical plane. The dotted lines aa′, bb′, etc., show the positions of the isobaric isothermal planes illustrated in fig. 8.

D. Isobaric section through the PTX model of the system Ab-C; this forms one side of the prism.

+ Ab, V + L and V + Ab, the pairs of phases which co-exist with a third phase if the bulk composition lies within the three-phase space V + L + Ab. The corners of the three-phase triangles give the compositions of V and L which can co-exist with crystals of Ab at different temperatures.

The field boundary (V +L)Ab is a vertical line through Ab, and the shapes of the other field boundaries will depend upon the properties of Ab, H_2O and C. If they are projected horizontally from Ab to the H_2O–C face of the prism, their relationships to each other are readily seen. Four possible forms of the projected field boundaries are illustrated in figure 6. These perspective TX projections show the proportions of H_2O and C in liquids or vapors on the field boundaries, without representing the proportion of Ab.

The liquidus and vaporus field boundaries may form loops ascendant or descendant from the ordinate representing the binary system Ab-H_2O, or there may be a maximum or minimum on the loop. The area within the loop is a projection of the three-phase space V + L + Ab, and above and below are projections of the two-phase spaces V + L[5] and V + Ab. Three-phase triangles are also represented; the sides (V)L + Ab and V(L)Ab of the three-phase triangles appear in figure 6 as points on the field boundaries, and the sides V + L(Ab) appear as horizontal lines connecting pairs of points. Since the sides of the triangles generate the two-phase surfaces, the series of points and lines representing the sides of the triangles trace the locus of these surfaces in projection; the surfaces (V)L + Ab and V(L)Ab thus coincide with the field boundaries (V)L(Ab) and V(L + Ab) respectively, and the surface V + L(Ab) coincides with the space V + L + Ab.

Orthogonal projection of the field boundaries from within the TX prism onto the base gives an isobaric polythermal equilibrium diagram. The four examples shown in figure 7 correspond to the four TX projections shown in figure 6. The proportions of the volatile components H_2O, C, and mixtures of H_2O and C dissolved in the ternary liquid are illustrated by the positions of the projected liquidus field boundaries and three-phase triangles in figure 7. The general shapes of the vaporus field boundaries in figure 7 were obtained by assuming that Ab is less soluble in that volatile component which is less soluble in the ternary liquid. The diagrams are schematic; the vaporus field boundaries should be much closer to the H_2O-C side-line.

The simple geometrical relationships illustrated in figures 6 and 7 are justified by the consideration of two chemical principles for ideal solutions: (1) ideally, the solubilities of volatile components in a liquid are inversely proportional to their vapor pressures, and (2) the freezing point of a liquid is depressed by the solution of a foreign substance, and the depression is greater the larger the quantity of substance dissolved. (See Findlay, 1951, for more detailed discussion.) Therefore, if the component C[6] has a higher vapor pressure than the component H_2O, and if conditions are ideal, then more H_2O will dissolve in the liquid than C and, at fixed pressure, liquid will exist at a lower

[5] It can be seen from figure 5C that the spaces L, and L+Ab also project onto the diagrams in figure 6. Our initial experimental work was completed in the presence of excess vapor, and only the spaces projected in figure 6 were intersected under these conditions.

[6] In the liquid phase.

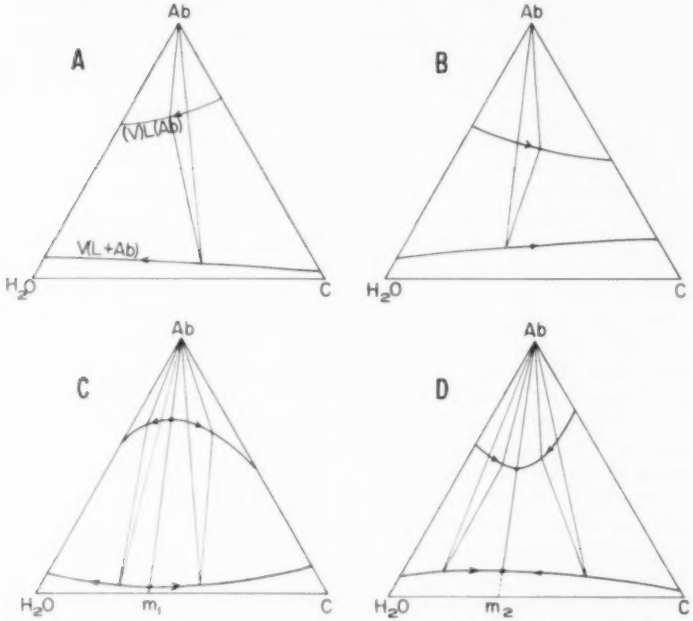

Fig. 7. Schematic isobaric polythermal equilibrium diagrams obtained by projecting field boundaries onto the base of the TX prism. The projected three-phase triangles show the disposition of tie-lines between liquids and vapors on the field boundaries. The four types illustrated in figs. A, B, C, and D correspond to those illustrated in fig. 6.

temperature in the system Ab–H_2O than in the system Ab–C. This condition is illustrated in figures 6A and 7A. Similarly, if the component C has a lower vapor pressure than H_2O, more will dissolve in the ternary liquid than H_2O and it will cause greater depression of the freezing point of Ab producing the conditions illustrated in figures 6B and 7B. The vapor in the ternary system will be richer in the more volatile component (i.e., the component with the higher vapor pressure) than the liquid with which it co-exists in equilibrium; this establishes the disposition of the three-phase triangles in projection.

If the liquid-vapor equilibria deviate from ideality, the relationships illustrated in figures 6C, 6D, 7C, and 7D may result. If the deviation from ideality is sufficient to produce a maximum or minimum on the (V)L and V(L) curves in the binary system H_2O-C at low pressures, it is not unlikely that this will be reflected in the ternary system, despite the fact that we are dealing with pressures and temperatures well above the critical curve for the binary two-volatile system.

If the system H_2O–C exhibits positive deviation there is an intermediate mixture of volatile components, m_1, which has a higher vapor pressure, at constant temperature, than either pure H_2O or pure C. Less of this combination of volatiles will probably dissolve in the ternary liquid than either H_2O or C,

and the shape of the field boundary (V)L(Ab) will be as shown in figure 7C. The liquid saturated with the mixture m_1 of H_2O-C at the pressure of the system will be in equilibrium with vapor and crystals of Ab at a temperature higher than the isobaric *invariant* condition in either of the systems Ab-H_2O and Ab-C, i.e., there will be a maximum on the field boundary (V)L(Ab), figure 6C. The compositions of vapors in equilibrium with any liquid and Ab will be given by a series of V + L(Ab) three-phase boundaries, the vapor being always richer than the liquid in the component with the higher vapor pressure, i.e., richer in the mixture m_1 (figs. 6C and 7C). At the maximum on the field boundaries the three-phase triangle reduces to a straight line, and here both vapor and liquid contain the same ratio of H_2O:C, m_1. The two field boundaries touch tangentially at the maximum in the TX projection (fig. 6C).

Similarly, if the system H_2O–C exhibits negative deviation, there is an intermediate mixture of volatile components, m_2, which has a lower vapor pressure than either pure H_2O or pure C, and more of this will dissolve in the ternary liquid than either H_2O or C. This will cause a greater lowering of the freezing temperature of the liquid, and there will be minima on the field boundaries. The solubility relations are shown in figure 7D, and the relative positions of the field boundaries, touching tangentially at the minimum in the TX projections, are shown in figure 6D. The V + L(Ab) three-phase boundaries will be directed away from the liquid with the lowest vapor pressure, i.e., the minimum melting liquid. The three-phase triangle at the minimum reduces to a straight line (fig. 7D).

Extreme positive deviation from ideality could presumably result in liquid immiscibility at some pressures, and critical phenomena could also intervene. In general, however, at the pressure used in the experiments to be described later, the field boundaries will resemble one of the types illustrated in figures 6 and 7. There are three groups: (1) boundaries passing regularly in temperature and composition from one binary to another, (2) boundaries with a maximum in temperature and minimum volatile solubility, and (3) boundaries with a minimum in temperature and maximum volatile solubility. In type (1) the boundary may pass from the equilibrium V + L + Ab for the system Ab-H_2O to higher or lower temperatures, depending upon whether the second volatile, C, is less or more soluble than H_2O.

Isobaric isothermal sections.—Although experimental data will be presented in the projections described above, the general phase relations may be more easily visualized by passing isothermal planes through the isobaric prism.

Figure 8 shows a series of isothermal sections through the ternary prism illustrated in figure 5. The lines aa′, bb′, cc′, dd′, and ee′ in figure 5C give the positions of the isothermal planes with respect to this vertical section through the prism.

At a temperature above the boiling point of Ab liquid (T_y in fig. 5C), an isothermal plane intersects the vapor space only (fig. 8A). Between the Ab melting temperature and boiling temperature (T_{Ab} and T_y in fig. 5C) the additional spaces L and V + L are intersected (fig. 8B). The space L + Ab appears below the melting temperature of Ab (fig. 8C). Two more spaces, V + L + Ab and V + Ab, are intersected between T_x of the binary system Ab-C

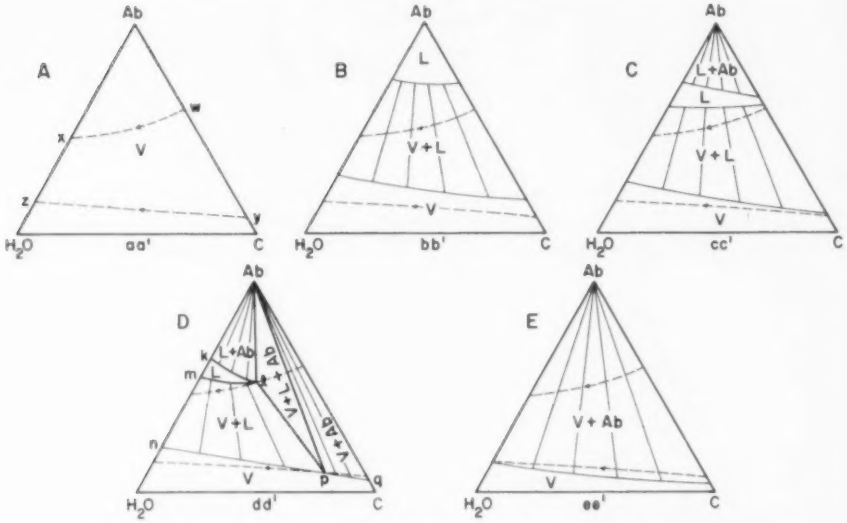

Fig 8. Schematic isothermal planes through the ternary isobaric prism illustrated in fig. 5. A, B, C, D, and E show the phase spaces, surfaces, and lines intersected by the planes at successively lower temperatures. The positions of the planes are given by the dotted lines aa′, bb′, cc′, etc., in fig. 5C.

and T_x of the system Ab-H_2O. The three-phase space is intersected in a three-phase triangle (fig. 8D). Isothermal planes in this temperature interval intersect six spaces and seven surfaces, which are labeled in figure 5C. The surfaces, intersected in curved or straight lines, extend through the prism from the side Ab-C-T to the side Ab-H_2O-T, and at successively lower temperatures, the isothermal three-phase triangle moves from Ab-C to Ab-H_2O (fig. 8D). At T_x for the system Ab-H_2O, the three-phase space reduces to the line V + L + Ab on the join Ab-H_2O, and at lower temperatures only the spaces V + Ab and V remain (fig. 8E). All two-phase spaces are filled with tie-lines, and the general arrangement of these is shown in the isotherms.

An isothermal plane intersects a field boundary at one point only. In figure 8D, the points *l* and *p* are the intersections of the field boundaries (V)L(Ab) and V(L + Ab) (compare the piercing point *l* in fig. 5C). However, the complete field boundaries are dotted in all diagrams as a guide for locating the positions of the phase sections as they change with decreasing temperature.

Figure 9 illustrates a series of isothermal planes, with temperatures decreasing from 9A to 9D, for a system with a maximum on both field boundaries (figs. 6C and 7C), and figure 10 illustrates isothermal planes for a system with a minimum on both field boundaries (figs. 6D and 7D). In these systems, an isothermal plane can intersect the field boundaries in two points. Further description is regarded as unnecessary. These isothermal planes, and the projec-

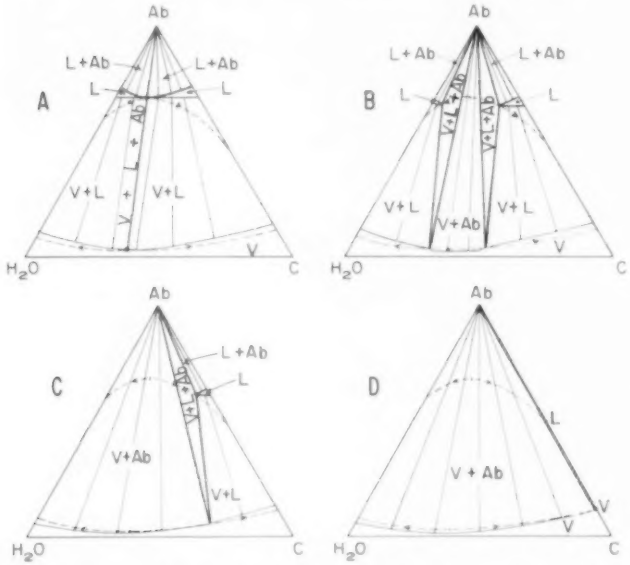

Fig. 9. Schematic isothermal planes through a ternary isobaric prism with a maximum on the field boundaries (fig. 6C and 7C). A, B, C, and D show the phase spaces, surfaces, and lines intersected by the planes at successively lower temperatures.

tions in figures 6C and 6D, should give the reader a good picture of the geometry of the ternary prisms.

For any bulk composition within the system, isothermal planes enable us to predict the changes in the equilibrium phase assemblage with falling temperature. For charges with compositions within the area Ab*wx* (fig. 8A) these are: V, V + L, L + Ab, V + L + Ab, and V + Ab; for charges within the area *wxyz* they are: V, V + L, V + L + Ab, and V + Ab; and for charges within the area CyzH$_2$O they are: V, and V + Ab. The isothermal planes also give information concerning the compositions of the phases present. At the temperature of the isotherm in figure 8D, Ab can be in equilibrium only with vapors on the line *pq*, with liquids on the line *kl*, or, if the bulk composition lies within the three-phase triangle, with liquid *l* and vapor *p*. In the area *klm* liquid exists alone, and liquids with compositions on the line *ml* can exist in equilibrium with vapors on the line *np*.

SYSTEMS CONTAINING H_2O AND CO_2

The authors have previously described the effect of H_2O and CO_2 on the melting temperatures of granite and feldspars (Wyllie and Tuttle, 1959). Qualitative results obtained were: (1) the rates of melting and crystallization of silicate mixtures in the presence of dry CO_2 are very slow, (2) dry CO_2 under pressure has little effect on the melting temperatures of granite and feldspars, and (3) in the presence of CO_2 and H_2O at fixed total pressure, the

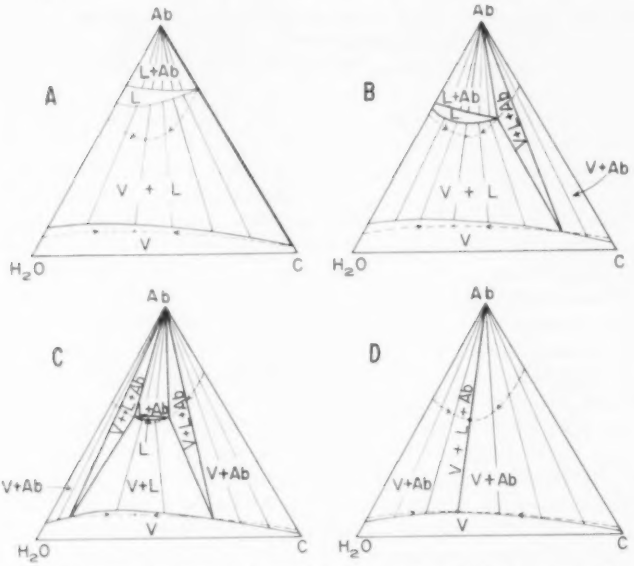

Fig. 10. Schematic isothermal planes through a ternary isobaric prism with a minimum on the field boundaries (figs. 6D and 7D). A, B, C, and D show the phase spaces, surfaces, and lines intersected by the planes at successively lower temperatures.

melting temperatures of granite and feldspars are raised when the proportion of CO_2 in the vapor phase is increased. From these results it was concluded that the solubility of CO_2 in granite and feldspathic liquids is less than that of H_2O. Moreover, results (1) and (2) suggest that the solubility of CO_2 is very low.

The system Ab-H_2O-CO_2 is therefore of the type illustrated in figures 5, 6A, 7A, and 8, where the second volatile C is CO_2. At a pressure of 2000 bars, the temperature T_x for Ab-H_2O is 845°C (fig. 5B), and the temperature T_x for Ab-CO_2 is probably greater than 1100°C (fig. 5D). The composition of the liquid in the three-phase equilibrium V + L + Ab for the system Ab–CO_2 at this pressure is very close to pure Ab.

One of the petrological applications of these results is the possibility that a hydrous granitic magma could be dehydrated when brought into contact with CO_2 released from a limestone by thermal metamorphism. Dehydration of the magma would induce crystallization, and could produce a quenching effect along the contact. The mechanism of this process can be illustrated by using the system Ab–H_2O–CO_2 as a model for the more complex "system" granite-H_2O–CO_2.

Consider an isothermal plane through an isobaric prism for the system Ab–H_2O–CO_2 at a temperature above T_x for Ab–H_2O (fig. 5, with C = CO_2). This will intersect the phase fields shown in Figure 8D (with C = CO_2). Let the magma be represented by a liquid within the one-phase space L, close to

the line *km* (fig. 8D). If CO_2 is added to the system at constant temperature and pressure, the composition of the liquid will move towards the CO_2 corner of the isobaric isothermal section. When the bulk composition crosses the line *lm*, the two phases V + L will co-exist, their compositions being given by the tie-line passing through the bulk composition. This means that H_2O has been displaced from the liquid into the vapor phase, i.e., the liquid has been partially dehydrated. Upon addition of more CO_2, the bulk composition will eventually move into the three-phase triangle, and when it does, Ab crystals will be precipitated from the liquid *l*, co-existing with vapor *p*. As more CO_2 is added, the liquid *l* is used up as crystals of Ab are precipitated, and vapor *p* is given off. When the bulk composition reached the line *p*Ab, only V + Ab remains. Thus, when CO_2 is added to the originally under-saturated liquid, the equilibrium sequence of events is: (1) a small amount of CO_2 dissolves in the liquid, (2) a vapor phase develops, and H_2O passes from the liquid into the vapor, and (3) Ab crystals are precipitated while H_2O and CO_2 are given off from the liquid until it is all used up.

For this process to go to completion in the schematic figure 8B, a very large quantity of CO_2 must be added to the original liquid. However, in the system Ab-H_2O-CO_2, the liquidus field boundary is more nearly parallel to Ab-H_2O (because the solubility of CO_2 in Ab liquid is very low), and for an isothermal plane with the point *l* closer to *km*, much less CO_2 would be required to produce complete crystallization.

In nature, of course, such a process would not occur at constant pressure and temperature, and it is difficult to imagine the addition of sufficient CO_2 to change the bulk composition of a body of granitic magma by so large an amount. Nevertheless, it is quite likely that near the margins of a granitic body, and in dykes emplaced in limestones, dehydration and rapid crystallization of the magma could occur in this way.

Another two-volatile system described by the authors is CaO-CO_2-H_2O (Wyllie and Tuttle, 1960). A ternary isobaric prism was determined experimentally at 1000 bars pressure. The geometry of this prism is complex, because the binary compounds $CaCO_3$ and $Ca(OH)_2$ are formed. Consequently, the prism contains six three-phase spaces, not one as in the examples described above. The geometry of this prism was described in detail, and the principles employed may be applied to silicate systems where compounds are formed between the silicate and the volatiles.

Part II of this series will describe experimental studies on the melting relations in the two systems $NaAlSi_3O_8$-H_2O-HF and $NaAlSi_3O_8$-H_2O-NH_3, together with results in "systems" containing granite.

References

Boeke, H. E., and Eitel, W., 1923, Grundlagen der Physikalisch-chemischen Petrographie: Berlin, Gebrüder Borntraeger.

Bowen, N. L., and Tuttle, O. F., 1950, The system $NaAlSi_3O_8$–$KAlSi_3O_8$–H_2O: Jour. Geology, v. 58, p. 489-511.

Findlay, A., 1951, The phase rule and its applications, 9th ed.: New York, Dover Publications, Inc.

Goranson, R. W., 1938, Silicate-water systems: phase equilibria in the $NaAlSi_3O_8$-H_2O and $KAlSi_3O_8$-H_2O systems at high temperatures and pressures: Am. Jour. Sci., v. 35A, p. 71-91.

Morey, G. W., 1957, The solubility of solids in gases: Econ. Geology, v. 52, p. 225-251.
Niggli, P., 1937, Das Magma und seine Produkte. I. teil: Physikalisch-chemische grundlagen: Akad. verglas. M. B. H., Leipzig.
Ricci, J. E., 1951, The phase rule and heterogeneous equilibrium: New York, D. van Nostrand Co. Inc.
Tunell, G., 1950, On the temperature-pressure-concentration diagram for binary systems in which only crystalline phases are the pure components: Am. Mineralogist, v. 35, p. 941-947.
Tuttle, O. F., and Bowen, N. L., 1958, Origin of granite in the light of experimental studies in the system $NaAlSi_3O_8$-$KAlSi_3O_8$-SiO_2-H_2O: Geol. Soc. America, Mem. 74.
Wyllie, P. J., and Tuttle, O. F., 1959, Effect of carbon dioxide on the melting of granite and feldspars: Am. Jour. Sci., v. 257, p. 648-655.
————, 1960, The system CaO-CO_2-H_2O and the origin of carbonatites: Jour. Petrology, v. 1, p. 1-46.

[American Journal of Science, Vol. 258, Summer 1960, P. 518-523]

LATE-GLACIAL AND POSTGLACIAL PLANT MACROFOSSILS FROM GILLIS LAKE, RICHMOND COUNTY, NOVA SCOTIA

W. B. SCHOFIELD and H. ROBINSON

Department of Botany, Duke University, Durham, North Carolina

ABSTRACT. An analysis of plant macrofossils in a deposit from Gillis Lake, Richmond County, Nova Scotia is compared with the pollen analysis from the same deposit. The macrofossils belong to aquatic or lake-shore genera or to trees with windborne seeds. Zones containing a variety of macrofossils from aquatic plants and lacking those from lake-margin species in other zones are interpreted to reflect a drier climate. Of the two birch species represented, a larger number or exclusive presence of *Betula lutea* seeds suggests a milder climate, whereas a larger representation of *B. papyrifera* suggests cooler conditions. Using these criteria, the macrofossil record largely supports the conclusions made from the pollen analysis. The water milfoil *Myriophyllum heterophyllum* is identified from fossil seeds. This species is presumably extinct in the present flora of Nova Scotia.

During their pollen analysis of a deposit from Gillis Lake, Nova Scotia, Livingstone and Livingstone (1958) set aside the macroscopic plant materials for later study. These specimens form the basis of the following report.

The only accurately identifiable materials from these collections were seeds and Charophyte zygotes. These were from aquatics or were wind-borne seeds from plants near the lake. The material, therefore, better reflects the lake flora than that of the surrounding country. From such scanty information it is impossible to make broad inferences, but taken in conjunction with the pollen analysis, the seeds serve to clarify a number of points.

The boring, 7 meters long, was made in the deepest part of the lake by means of a 2-inch Livingstone sampler. The cores were split in half longitudinally, and twelve samples, each consisting of one-third or one-half meter of the split 2-inch core, were found to contain seeds. The seeds were extracted by suspending each sample in a solution of 10 percent HNO_3 as suggested by Godwin (1956). Seeds were removed when they floated to the surface of the solution. Stirring the mixture allowed seeds to rise more easily, and after several hours the residue was strained through a fine mesh screen to recover material that had not floated to the surface of the liquid. The fossil seeds were compared with samples from dried plants in the Duke University Herbarium.

The following discussion of the samples proceeds from the oldest to the youngest.

From the pollen record, zone L1 was interpreted to have represented an open vegetation of a tundra nature. The macrofossils are entirely of submerged aquatic species (*Chara*, *Nitella* and *Potamogeton berchtoldi*), neither contradicting nor supporting the pollen record.

Zone L2 samples revealed no macrofossils. The pollen record of the zone shows a high proportion of *Betula* (birch) and *Alnus* (alder) pollen with other species, except of Cyperaceae and *Artemisia*, barely represented. This record was interpreted to suggest a warming of climate and a closing of the vegetation.

Zone L3, interpreted from the pollen record to have developed during a return of the vegetation to a more open type, showed only a single *Potamogeton* seed. As far as it goes, this agrees with the L1 sample which has also been considered to represent open vegetation. A radiocarbon sample (Y-524, 10,160 ± 160 yr.) came from this zone in this meter-sample (Deevey, et al., 1959).

Zone A1 contains the earliest records of both *Betula papyrifera*, paper birch (3 seeds) and *B. lutea*, yellow birch (1 seed). This is in conjunction with a pollen record indicating a closed boreal type forest (increased *Betula* and *Picea*, spruce). Livingstone and Livingstone considered that drier climate might be responsible for the small proportion of *Abies* (fir) pollen. Perhaps as another indication of dryness is the presence of seeds of lake-margin plants (*Carex* and *Myrica gale*), whereas only submerged aquatics are represented in older strata. The number of aquatics, though large in comparison to the lower strata, is still relatively low. The presence of seeds of the aquatics *Nuphar*, *Nymphaea odorata* and *Najas flexilis* suggests warmer conditions than in the previous periods.

The bottom half of the fourth meter, consisting largely of zone A2 and part of B, shows *Betula papyrifera* as the only birch and, in addition, a few submerged (*Nuphar*, *Nymphaea odorata* and *Najas flexilis*) and lake-margin plants (*Scirpus* and *Carex*). The pollen diagram showed a continuation of high *Betula* percentages and the appearance of *Quercus* (oak) in small but increasing proportion, suggesting a somewhat warmer climate.

The top half of the fourth meter, containing the rest of zone B and most of zone C1, exhibits a conspicuous representation of *Betula papyrifera* with only a single seed of *B. lutea*. The *Betula* pollen was diminishing in proportion during the period. Thus, while *Betula* becomes much more prominent among the seeds, the pollen indicates a rise of *Pinus* in the B zone. The hardwood forest indicated by the C1 pollen apparently was better developed than at present and possibly indicates a warmer climate. Lake-margin plants are represented by the sedge genus *Cladium*, the bur-reed *Sparganium*, and the dewberry *Rubus pubescens*.

The lower third of meter three, containing the top of zone C1 and part of C2, shows a reduction in the seeds of *Betula papyrifera* to equal the number of *B. lutea* seeds. This is correlated with a continuing decline of *Betula* pollen. The shift in aquatics toward submerged types, including the reappearance of the charophytes *Chara* and *Nitella*, implies the beginning of a generally more humid period.

The middle of the third meter, consisting of most of zone C2, contained comparatively few seeds. Shore plants are absent, except for three *Betula lutea* seeds. This might be the result of maximal humidity indicated by the peak in hemlock pollen.

In the upper third of meter three, composed of a small portion of zone C2 and the lower half of C3a, eighteen seeds of *Betula lutea* were found, but none of *B. papyrifera*. The pollen of this stratum shows diminished pine and hemlock proportions and a third rise in the percentage of *Betula*. The presence of a single *Picea* seed at a time of very low proportions of *Picea* pollen seems to

be anomalous. Other seeds represent a variety of submerged aquatics: *Nuphar*, *Nymphaea odorata*, *Najas flexilis*, *Potamogeton berchtoldi* and *Myriophyllum heterophyllum*. *Sparganium* is the most marginal of the aquatics included. This represents a trend toward increased abundance of lake-margin plants not shown in the next lower level.

The bottom half of the second meter, including the top of zone C3a and the bottom quarter of C3b, apart from showing a smaller variety of seeds than the preceding stratum, fails to differ from it in any important respect in the seed or pollen records. Eighteen seeds of *Betula lutea* and seeds of *Sparganium*, *Nuphar*, *Nymphaea odorata* and *Myriophyllum heterophyllum* were found.

The top half of the second meter, consisting entirely of part of zone C3b, shows a reduction in the number of *Betula lutea* seeds. Although possibly of no significance, when considered in conjunction with the reappearance of *B. papyrifera* in the next higher meter it may indicate a shift toward a cooler climate. The occurrence of *Nuphar*, *Nymphaea* and *Sparganium* agrees with adjacent strata. Two seeds of *Myriophyllum heterophyllum* were found in this sample. This species, present also in the two preceding strata, is not reported from Nova Scotia by Roland (1945). One seed of *Potamogeton epihydrus*, the commonest pondweed in the present flora of Nova Scotia, is named from this level. Although not listed for previous strata, other poorly preserved *Potamogeton* seeds from lower levels could belong to this species.

The macrofossils from the uppermost meter were all kept in one sample and thus no distinction can be made between the two zones included. The larger part of the meter was from the top of zone C3b in which the pollen is similar to that of the next lower sample. In the thin C3c zone *Betula* pollen is noticeably diminished in proportion and *Picea* and *Abies* increase slightly but distinctly. Only five *Betula lutea* seeds were found in the layer while *B. papyrifera* reappears with two seeds. The aquatics include the usual *Nuphar* and *Nymphaea odorata*. A seed of *Potamogeton epihydrus* indicates the continued presence of this extant member of the Nova Scotia flora. A seed of *Sagittaria cuneata* (arrowhead) was also recovered from this level. On the basis of the changed proportion of *Betula* seeds the climate during the period represented here probably became generally cooler, as is also indicated by the C3c pollen record.

The following is a list of the samples from the youngest to the oldest showing their plant macrofossil contents:

Species	Number	Species	Number
First meter			
Betula lutea	5	*Nymphaea odorata*	14
B. papyrifera	2	*Potamogeton epihydrus*	1
Nuphar	10	*Sagittaria cuneata*	1
Top half of second meter			
Betula lutea	7	*Nymphaea odorata*	5
Myriophyllum heterophyllum	2	*Potamogeton epihydrus*	1
Nuphar	2	*Sparganium*	2
Bottom half of second meter			
Betula lutea	18	*Nuphar*	4
Myriophyllum heterophyllum	1	*Nymphaea odorata*	11
Najas sp. ?	2	*Sparganium*	2

Species	Number	Species	Number
Top third of third meter			
Betula lutea	18	*Nymphaea odorata*	15
Myriophyllum heterophyllum	1	*Picea (mariana-rubens)*	1
Najas flexilis	1	*Potamogeton berchtoldi*	1
Najas sp. ?	4	*Sparganium*	4
Nuphar	10		
Middle third of third meter			
Betula lutea	3	*Nuphar*	1
Najas flexilis	1	*Nymphaea odorata*	15
Bottom third of third meter			
Betula lutea	2	*Najas* sp. ?	8
B. papyrifera	2	*Nuphar*	3
Chara	1	*Nymphaea odorata*	21
Nitella	1	*Scirpus*	1
Top half of fourth meter			
Betula lutea	1	*Nymphaea odorata*	9
B. papyrifera	13	*Potamogeton* sp.	1
Cladium mariscoides	1	*Rubus pubescens*	1
Najas sp. ?	7	*Sparganium*	2
Nuphar	7		
Bottom half of fourth meter			
Betula papyrifera	5	*Nuphar*	2
Carex	1	*Nymphaea odorata*	14
Najas flexilis	3	*Scirpus*	1
Top of fifth meter (A1)			
Betula lutea	1	*Najas flexilis*	2
B. papyrifera	3	*Nuphar*	1
Carex	1	*Nymphaea odorata*	1
Myrica gale	2		
Bottom of fifth meter (L-3)			
Potamogeton sp.			
Sixth meter (L-2)			
Top two thirds of seventh meter (L-1b)			
Potamogeton sp.	2		
Bottom third of seventh meter (L-1a)			
Chara	2	*Potamogeton berchtoldi*	1
Nitella	35		

DISCUSSION

Vegetational changes of short duration or effects of differential rates of plant migration are obscured by the long periods (at least a thousand years) that must be represented by most of the samples. Nevertheless, correlation of the macrofossil record with the interpretation of the pollen record (Livingstone and Livingstone, 1958) strongly indicates some general climatic and floristic trends.

Absence of tree seeds and of lake-margin herbs within the lower strata, though negative evidence, does not contradict the indication of the pollen record that these strata were laid down in a time of open vegetation, possibly tundra in nature.

Of three periods showing an increased proportion of *Betula* pollen, the first was part of the late-glacial time of predominantly herbaceous vegetation; no seeds were found in deposits of this time. The second increase coincided with a period of *Betula papyrifera* seed predominance, which suggests that the pollen, too, was from that species. The third and longest period of abundant *Betula* pollen was marked by a predominance of *B. lutea* seeds, with *B. papyrifera* occurring only in the uppermost meter. Thus the third pollen rise seems likely

to have been due to *B. lutea*. The zone lacking seeds of *B. papyrifera* matches the period interpreted as warmer than the present, on the pollen evidence.

Within the warmer period the pollen record reveals indications of two relatively dry periods and an intervening more humid stage. Coincident shifts can be noticed among the aquatic macrofossils: two periods of numerous lake-margin plants being separated by a stage when only submerged aquatics were represented. A period of greater humidity may have raised the water level, so that the shores of the lake were farther from the point of sampling. Conversely, in drier periods, closer proximity of the lake margins could have increased the number of seeds from shore plants in the sampled portion of the lake. On this interpretation, the climatic changes indicated by the pollen record are reinforced by the seed record.

The macrofossils, as can be seen in the table, tend to reflect the fraction of vegetation that falls under the immediate influence of the lake. The special character of this flora is accentuated by the persistence of relict species for which the regional climate has become unfavorable. Differences between the seed and the pollen records could result from this fact.

ACKNOWLEDGMENTS

We wish to thank Dr. D. A. Livingstone for his original suggestion of the study and for help during the identification of the material and preparation of the manuscript. We are grateful to Dr. R. L. Wilbur, Curator of the Duke University Herbarium, for his cooperation.

REFERENCES

Deevey, E. S., Gralenski, L. J., and Hoffren, V., 1959, Yale Natural Radiocarbon Measurements IV: Am. Jour. Sci. Radioc. Supp., v. 1, p. 144-172.

Livingstone, D. A., and Livingstone, B. G. R., 1958, Late-glacial and postglacial vegetation from Gillis Lake in Richmond County, Cape Breton Island, Nova Scotia: Am. Jour. Sci., v. 256, p. 341-359.

Roland, A. E., 1945, The flora of Nova Scotia: Nova Scotia Inst. Sci. Proc., v. 21, no. 3, p. 1-552.

Figs. 1-29. Plant macrofossils from Gillis Lake, N. S. (Scale: Figures 6, 8, 13 & 15 ×165, all other figures ×5.) 1. *Betula papyrifera* seed. 2-3. *B. lutea* seeds. 4. *Picea* (*mariana-rubens*) seed. 5. *Nuphar* seed. 6. *Nuphar*, cellular structure of seed-coat. 7. *Nymphaea odorata* seed. 8. *N. odorata*, cellular structure of seed-coat. 9. *Rubus pubescens* seed. 10. *Myriophyllum heterophyllum* seed. 11-12. *Najas flexilis* seeds. 13. *N. flexilis*, cellular structure of seed-coat. 14. *Najas* sp. ? seed. 15. *Najas* sp. ?, cellular structure of seed-coat. 16. *Sparganium* seed. 17. *Sparganium*, cross-section through body of seed. 18. *Cladium mariscoides* seed. 19. *Potamogeton epihydrus* seed. 20. *Potamogeton* sp. seed. 21. *P. berchtoldi* seed. 22. *Sagittaria cuneata* seed. 23. *Myrica gale* seed. 24. *Scirpus* seed. 25. *Carex* seed. 26. *Nitella* zygote. 27. *Chara* zygote. 28. Bryozoan statoblast. 29. Unidentified animal fossil.

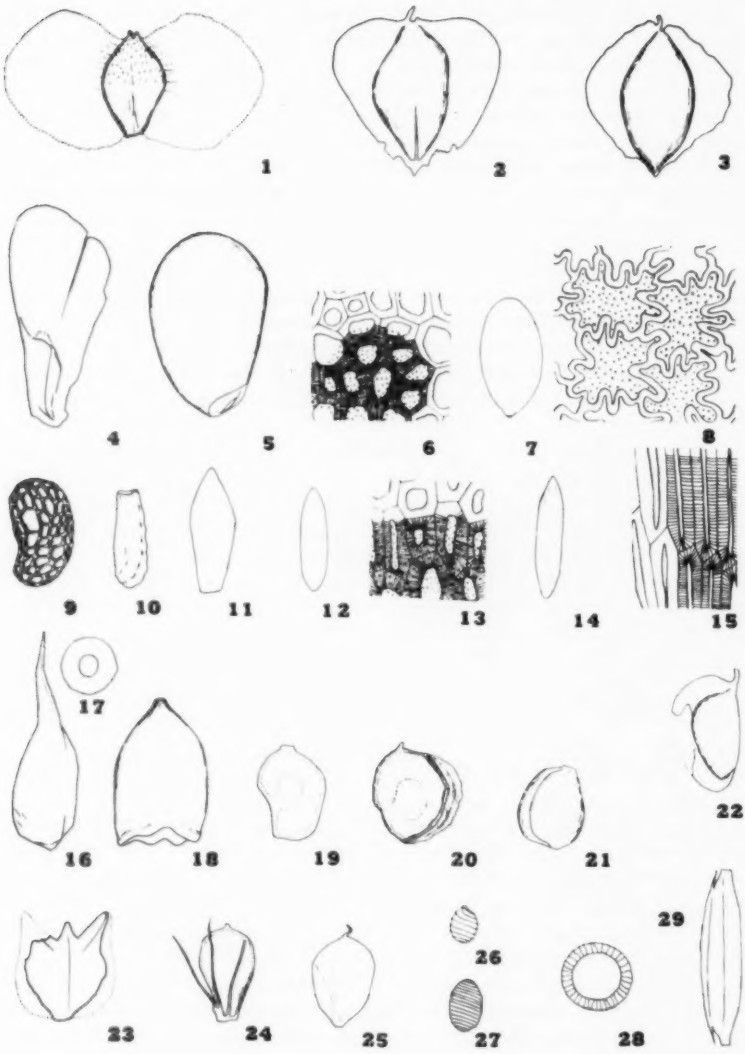
1
2
3
4
5
6
7
8
9
10
11
12
13
14
15
17
16
18
19
20
21
22
23
24
25
26
27
28
29

REVIEWS

Soils for the Archaeologist; by I. W. CORNWALL. P. 230. New York, 1958 (The Macmillan Company, $7.50).—Despite its title, this book should really be called Soils for the British Archaeologist or, at best, Soils for the European Archaeologist. The author uses Kubiena's classification for the soils of Europe, based on the concept of soil type, in which an attempt is made to classify soils according to schemes employed in the natural sciences. Each one of these types is rather broadly defined, and for the archaeologist who is usually more involved with the problems of topography, drainage, and vegetation at a particular site, it would appear that the concept of soil series, which is based on these factors, would be more useful. The author neglects to state that there is still much argument among soil scientists as to what is a meaningful classification scheme. There is no mention that soil classification is a problem, and that a scheme covering all the soils of the world without regard for national boundaries is really what would be most useful for an archaeologist who becomes involved with this problem. In fact, Cornwall states that the scheme of Kubiena "for the present purpose is of unnecessarily wide geographical scope . . . ", thus implying that his book is primarily intended for the British archaeologist only. The author also tends to oversimplify the problems of soil profile development and the possible conclusions that can be drawn from its study.

The discussion of the problems of sampling is not statistically sound. For example, it is much safer statistically to take a large number of small samples of a given layer than to, as the author suggests, take one large sample. Actually, no matter how small an area is to be sampled, one large sample will rarely be adequate to give a reliable answer to the question being asked. No valuable discussion is presented on the problems of mixing samples, although it is stated that the "proof of a good determination is its repeatability". Unfortunately, this rather important concept is mentioned only under the section concerned with sampling and is not again emphasized in the rest of the book.

It is also suggested that texture analysis be accomplished by "feel". For the archaeologist, this is hardly a useful concept since textural analysis of this type takes a number of years of experience. A mechanical analysis of the sample leaves little doubt as to what the particle size distribution of the sample actually is.

Cornwall states in his section on chemical methods that "great accuracy in determination of any constituent is not only unnecessary in many circumstances—it may be positively misleading". It is true that in checking comparisons between soil horizons the relative differences are what is important but they should be as accurate as possible. This is especially true since these methods are being prepared for use by the chemically untrained.

The author implies that this book is written primarily for those with an humanistic rather than scientific training, yet he uses the language of chemistry without explanation, gives no basic methods for calculating the percentages of a given element in a given sample, neglects to discuss the problems of the variability of water (distilled and rain) throughout the world, and presents no discussion on the difficulties of obtaining chemically pure dishes or

the fact that soap and detergents frequently contain more of a given element than the sample being tested.

A number of difficulties arise in the information presented concerning the determination of pH. The first is that of the ratio of soil to water. Varying results are obtained for varying ratios. The range that has been investigated in this country is from that of a paste to 1:2.5. Cornwall suggests the use of 1:15. Secondly, the usual procedure is to stir the mixture of soil and water frequently over a period of half an hour in order to allow the solution to attain equilibrium prior to the pH determination. Cornwall recommends that the soil and water mixture be stirred and the hydrogen ion concentration determined immediately. This suggestion creates some difficulty since replicability is not often obtained by this method.

A number of methods are presented for organic matter determination in soils. The author dislikes the dichromate oxidation methods since, he states, they have the disadvantage of oxidizing ferrous iron to ferric iron which is then included in the subsequent determination. The rather effective use of a complexing agent for iron, such as sodium fluoride, to eliminate this error is not mentioned. He suggests the alkali soluble method which unfortunately is not widely enough used to allow the archaeologist to compare his results with those obtained by study of the area surrounding the site. The use of peat as a standard in this method also creates some error.

Cornwall states that he has no experience in the determination of nitrogen. Unfortunately he neglects to mention the empirical relationship between organic matter and nitrogen which would enable the archaeologist to obtain a comparative idea of how much nitrogen his sample contains by determining its organic matter content.

Phosphorus is of great interest to the archaeologist, since its determination gives some indication of occupation. However, Cornwall does not mention some of the difficulties that one is likely to encounter in the method presented, such as the interference of silica and the fact that filtration must be accomplished with extreme care lest soil particles of colloidal size present in the filtrate increase the subsequent colorimetric reading.

Generally speaking, if the methods presented are going to be employed by the archaeologist, it would appear advantageous for him to use methods that are being used in the area of his work so that he might have a basis of comparison and be able to determine whether or not the data he has obtained from his site is significantly different from the surrounding area.

The author endeavors to accomplish too much. He implies, with rare exceptions, that the problems of agronomy are solved, although he does mention that organic matter is not too well understood. This in turn tends to produce a kind of shaman attitude on the part of the archaeologist toward the soil scientist. However, in the preface, Cornwall states that he wishes to remove the "witch-doctor" aura from the soil scientist. Possibly he runs the risk that, in correcting the impression that laboratory work is so occult that the results must be profound, he creates the impression that it is all so simple that interpretation is never difficult, thus leading back again to the uncritical acceptance of laboratory results.

URSULA M. COWGILL

Basic Geology for Science and Engineering; by E. C. DAPPLES. P. 609. New York, 1959 (John Wiley & Sons, Inc., $9.50).—It is difficult to review a textbook such as this without considering the nature of the course for which it is intended. The title of the book immediately implies exclusion from comparison with the many textbooks written for use in elementary college geology courses. The intent has been (p. 7),

> . . . the presentation, under the title of basic geology, of a series of interrelated subjects of principal concern to the student of science and engineering.

Information is presented in a detailed, thorough manner that presupposes students familiar with algebraic and statistical notation, fundamentals of chemistry and physics, and the interpretation of diagrams as complex as classification tetrahedra for igneous rocks (p. 114-115) and curves of particle-size frequency distribution (p. 28 and following). Stokes' law (p. 125) and Darcy's law (p. 307) are derived. Solution and precipitation of carbonate minerals by ground water are discussed in terms of ionic equilibria equations (p. 340).

A discussion of soil materials, including a thorough description of particle size distribution in sediments, is introduced in the first pages of this text. Successive chapters concern the physical and chemical properties of rocks and rock-forming minerals. Thus the author encompasses the first of the three general sections of his book: earth materials, processes of erosion and deposition, and processes of crustal deformation and metamorphism.

Under the heading "soil-forming processes", rock weathering is next considered in detail. A 74-page chapter on streams and shorter chapters on shoreline processes, ground water, wind deposits, processes associated with glaciation, and sedimentary rocks complete the consideration of processes of erosion and deposition. Crustal deformation and metamorphism are described in concluding chapters. About 65 percent of the text is devoted to consideration of the processes of erosion and deposition.

"Basic Geology" was referred to by the reviewer during a one-semester introductory course in physical geology. The book provided a wealth of source material for lectures, and was found to summarize recent technical progress in a wide range of fields. As a teachers' source book, the volume is to be commended.

The use of this book as a text would raise certain problems, primarily of organization. The independent treatment of materials and processes has resulted in repetition which, although perhaps pedagogically valuable, restricts a teacher in the sequence of presentation. For instance, soil varieties are described on page 9-17, with useful maps of the major soil regions of the world and of the United States, but a discussion of the soil profile and processes of soil formation is deferred until page 160-168. The reviewer has not found it possible to describe the podzolic and red-yellow soil types of the U. S. without discussing the processes by which these soil types form.

Another example of complex organization was noted in the chapter entitled "Shoreline processes". Under that heading is included subjects as diverse as continental shelves, waves and currents, thermal stratification in lakes, organisms of fresh-water lakes, bog formation, and saline lakes. Thus aquatic biology, lacustrine sediments, and evaporite deposition are some of the topics

rather surprisingly included under a seemingly conventional chapter heading.

The chapter on crustal deformation, although short in comparison to the consideration of erosional and depositional processes, contains a description of primary rock structures (p. 504-513) which are defined as those not produced through later deformation. It would seem that the primary structures should have been described in context with the rock type involved.

The author of this book notes in his preface that tables and graphs have been used wherever feasible. This is commendable if not carried to extremes, but the reviewer could not admit as useful such illustrations as table 2.5 (p. 40) which summarzies the significant [sic] attributes of ideal bedrock types (igneous rock colors; light gray, dark gray, black or red: sedimentary rock colors; light gray, green gray, blue gray, dark gray, red, or brown: metamorphic rock colors; green gray, mottled gray, dark gray, brown gray) or table 7.3 (p. 244) which attempts to characterize features of various physiographic stages in terms of selected geomorphometric measurements. The latter table is a compilation of widely overlapping numerical values rather arbitrarily assigned to several stages in the cycle of erosion.

Very few typographical or editorial errors appear to have crept into this book. Feldspars are endowed with a third cleavage direction on page 72, figure 10.19 is referenced rather than figure 10.16 on page 165, and an indexed reference to the term "unconformity" does not appear on page 236. The author used an obviously dated source for estimates of the duration of Pleistocene stages on page 434, although elsewhere in the chapter on glaciation he cited much more recent references.

The fundamental issue is the question of what is important in a "Basic Geology" text. Dapples apparently feels that a thorough understanding of sedimentology and sedimentary rocks is vital to the geological training of a future engineer or scientist. But to dismiss the concept of time-rock units with the statements, "with few exceptions the engineer is not concerned with time-rock groupings . . . ." (p. 496) and "from an engineering point of view, however, they are not of particular importance . . . " (p. 497) is to deny the future engineer the broadening experience of geology. Attempts to quantify the technical aspects of geology are important and useful, but the reviewer wonders if this is the matter for "Basic Geology".

ARTHUR L. BLOOM

Introduction to the Theory of Sound Transmission; by C. B. OFFICER. P. viii + 284; 191 figs. New York, 1958 (McGraw-Hill Book Co., Inc., $10.00). —This book provides a good foundation for those interested in theoretical research in the field of underwater acoustic propagation. The mathematics involved (which makes up a large part of the book) will probably be quite difficult for a senior undergraduate student, suggested by the author as part of his audience; however, an understanding of the material covered will give the reader the background necessary for research in this field.

The first chapter contains an introduction to simple acoustic wave theory. This is followed by a chapter on the development of general transmission theory. The ray theory approximation is derived, and applied to refraction of

rays in media of varying sound velocity; both sound intensity and travel time calculations are illustrated. A discussion of normal modes, Fourier analysis of transient waves, and simple reflection problems is included. Shallow-water and deep-water transmission of acoustic waves are next treated; these chapters give a detailed analysis of the techniques used in solving the important propagation problems. Each begins with a short discussion of the oceanography applicable to that portion of the ocean under consideration; ray theory and wave theory solutions are then developed and interpreted. The final chapters are on the reflection of waves from different types of boundaries and on sound attenuation due to absorption and scattering.

Although a familiarity with complex variable theory is necessary, the author does give many of the fine details of his mathematical developments (too detailed in many places, where algebraic manipulation is carried out "step-by-step"). The many graphs and illustrations do much to make the text understandable. In all, this is a good introduction to underwater sound theory, and will also serve as an illustration of the use of advanced mathematical techniques in solving boundary value problems. DAVID MINTZER

The Upper Atmosphere; by H. S. W. Massey and R. L. F. Boyd. P. xii + 333. New York, 1959 (Philosophical Library, $17.50).—Among the features which make this book noteworthy are its authoritative authorship and the fact that it is written for readers with only an elementary knowledge of physics and mathematics. The importance of the subject need not be stressed today. There are descriptive chapters detailing the structure and properties of the atmosphere, tides, magnetic effects and the lights in the night sky. The methods of probing the atmosphere with sound and radio waves are explained, and a good deal of space is devoted to disturbances, meteors and cosmic rays. I have found the presentation of the material and the organization of the book truly excellent, the numerous illustrations enlivening and helpful. Physicists, geologists and space technologists will find this book most useful; unfortunately, the price is very high. HENRY MARGENAU

Publications Recently Received

Marine Boring and Fouling Organisms; edited by Dixie Lee Ray. Seattle, 1960 (University of Washington Press, $8.50).

The Edge of Objectivity; by Charles Coulston Gillispie. Princeton, 1960 (Princeton University Press, $7.50).

Electronic Computers, Principles and Applications, 2nd ed.; by T. E. Ivall. New York, 1960 (Philosophical Library, $15.00).

Search for the Past; by James R. Beerbower. New York, 1960 (Prentice-Hall, Inc., $7.50).

The Origins of Modern Science; by Herbert Butterfield. New York, 1960 (The Macmillan Co., $1.25).

The Logic of Modern Physics; by P. W. Bridgman. New York, 1960 (The Macmillan Co., $1.25).

Principles of Paleobotany, 2nd ed.; by William C. Darrah. New York, 1960 (The Ronald Press Co., $6.50).

Principles of Petroleum Geology, 2d ed.; by William L. Russell. New York, 1960 (McGraw-Hill Book Company, Inc., $9.50).

Biological and Medical Electronics; by Ralph W. Stacy. New York, 1960 (McGraw-Hill Book Company, Inc., $9.50).

VOL. 258 No. 7, 1960

American Journal of Science

SUMMER 1960

CONTENTS

Compositional Characteristics and Equilibrium Relations in Mineral Assemblages of a Metamorphosed Iron Formation
Robert F. Mueller 449

Experimental Investigation of Silicate Systems Containing Two Volatile Components, Part I. Geometrical Considerations
P. J. Wyllie and O. F. Tuttle 498

Late-Glacial and Postglacial Plant Macrofossils from Gillis Lake, Richmond County, Nova Scotia ....*W. B. Schofield and H. Robinson* 518

REVIEWS

Soils for the Archaeologist; by I. W. Cornwall .....*Ursula M. Cowgill* 524
Basic Geology for Science and Engineering; by E. C. Dapples .....*Arthur L. Bloom* 526
Introduction to the Theory of Sound Transmission; by C. B. Officer ....*David Mintzer* 527
The Upper Atmosphere; by H. S. W. Massey and R. L. F. Boyd ....*Henry Margenau* 528
PUBLICATIONS RECENTLY RECEIVED 528